Arch Appl Mech (2018) 88:141–173
https://doi.org/10.1007/s00419-017-1296-z

SPECIAL

C. B. Silbermann · J. Ihlemann

Geometrically linear continuum theory of dislocations revisited from a thermodynamical perspective

Received: 7 January 2017 / Accepted: 14 August 2017 / Published online: 20 September 2017

Abstract Continuum dislocation theory (CDT) allows the consideration of dislocation ensembles by introducing the dislocation density tensor. Though the kinematics of geometrically linear CDT are well established, the closure of governing field equations is not finished yet. The present study now brings together different principles for such a closure: It is shown how the field equations for the CDT can be obtained from potential energy minimization and from the phase field approach. These two energetic methods are integrated into a generic thermodynamic framework with twofold benefit: First, the rigorous thermodynamic treatment allows clarifying physical consequences of the energetic methods, among them the proof of thermodynamic consistency. Second, the framework provides a basis for consistent extensions of CDT. In this way, a new dynamic formulation of CDT is presented, which enables the analysis of the evolution of dislocation structures during plastic deformation. Moreover, a variety of possible dissipative phenomena is considered and the mechanical balance laws are deduced. For two special cases, the field equations are derived in the strong form and the stability of the solution is analyzed. Next, a flexible numerical solution algorithm is presented using the finite difference method. Solutions of various initial boundary value problems are presented for the case of plane deformations. Therefore, some of the dissipative phenomena are further investigated and two distinct sources of the Bauschinger effect are identified. Special attention is also given to different boundary conditions and their effect on the solution. For the case of uniaxial compression, the numerical results are confronted with experimental data. Thus, the simulations are validated and a new consistent interpretation of the experimental results is achieved.

Keywords Dislocations · Dislocated crystal · Continuum theory · Dissipation · Phase field method · Finite difference method

1 Introduction

The mechanical behavior of crystals, especially metallic ones, strongly depends on the underlying defect structure. For a broad class of metals, it is the motion of dislocations that carries the plastic deformation, and new macroscopic properties emerge from the collective self-organization of dislocations [2,9,17,46,60].

Electronic supplementary material The online version of this article (doi:10.1007/s00419-017-1296-z) contains supplementary material, which is available to authorized users.

C. B. Silbermann (✉) · J. Ihlemann
Institute of Mechanics and Thermodynamics, Chair of Solid Mechanics, Chemnitz University of Technology, Reichenhainer Straße 70, 09126 Chemnitz, Germany
E-mail: christian.silbermann@mb.tu-chemnitz.de
Tel.: +49-371-531-38845
Fax: +49-371-531-838845

As large dislocation ensembles are involved in typical pattern formation processes, a *continuum* dislocation theory (CDT) is required. At the moment, there are many competing CDTs (for a comprehensive overview, see, e.g., [47,58]) which all have in common that gradients of macroscopic plastic deformation are related to the presence of geometrically necessary dislocations (GNDs). Therefore, the plastic distortion is introduced as an additional primary field variable.[1] In order to take into account *all* dislocations, some theories consider statistically stored dislocations (SSDs) [3] as well, e.g., [22].

The present study adopts the CDT proposed in [5] and developed further in a series of papers [6,25, 26,36,37,39,40]. Essentially, this is the so-called curl(H_p)-Model of strain gradient plasticity [15]. The main advantage of this approach is its clear and relatively simple structure. As a key assumption, the curl of the plastic distortion—the dislocation tensor—is considered as a thermodynamic state variable which reflects tensorial dislocation properties. Using the example of discrete dislocations, this is reviewed briefly in Sect. 2. For (large) dislocation ensembles the resulting dislocation tensor represents a homogenized quantity characterizing the effect of GNDs. Thus, both the macroscopic strain energy of the deformed crystal and the elastic energy of (geometrically necessary) dislocations can be captured. Based on that, Sect. 3 provides two energetic methods for the derivation of field equations. Section 4 then integrates these approaches into a comprehensive and consistent thermodynamical framework. Thereby, the dissipation of energy due to dislocation motion can be introduced in a thermodynamically consistent fashion. Furthermore, it is shown how the usage of a dissipation potential facilitates the modeling of very different dissipative phenomena. As a new feature, it is demonstrated how to arrive at a dynamical theory, which is formally identical to the phase field method. This enables the analysis of the evolution of dislocation structures during plastic deformation. For the special case of a continuously dislocated single crystal with one active slip system, the governing field equations are derived explicitly in Sect. 5. Moreover, a micromechanical interpretation for specific forms of the dissipation potential is given. Section 6 then presents numerical solutions of the corresponding initial boundary value problems for the case of plane deformations. To this end, an in-house simulation code using the finite difference method is adopted. The value of the simulation results is estimated by a validation on experimental data. To this end, a series of uniaxial plane strain compression tests on Cu single crystals serves as a reference. Finally, Sect. 7 discusses the presented extension of the theory, indicates existing challenges and problems and motivates directions for future research.

For the sake of compact and clear representation, symbolic tensor notation is preferred throughout this paper. Tensors of nth order are denoted by a small or capital letter with n underscores, e.g., $\underline{\underline{U}}$ is a second-order tensor. The tensor product is denoted by $\otimes$, the cross product is denoted by $\times$, and the nth contraction of tensors is written symbolically with n $\cdot$ -dots. The coefficients with respect to a certain Cartesian coordinate system $\underline{e}_a$ are $U_{ab} = \underline{e}_a \cdot \underline{\underline{U}} \cdot \underline{e}_b$. The arrangement of second-order tensor coefficients in a quadratic matrix is denoted by $[U_{ab}]$. The circulation and divergence theorem are used in order to define consistent (right) differential operators such as Gradient grad, Divergence div and Curl curl. Whenever it facilitates reading, those operators are also expressed symbolically with the Nabla operator denoted by $\underline{\nabla}$. A short overview of tensor calculus and analysis is given in "Appendix A."

2 Kinematics of a continuously dislocated crystal

Within CDT, the dislocation (density) tensor is a thermodynamic state variable, which reflects tensorial dislocation properties and allows the consideration of large dislocation ensembles. Using the example of discrete dislocations, this section briefly reviews basic dislocation properties and how they are captured by the dislocation tensor.

2.1 Characteristics of single dislocations

Dislocations are line-shaped crystal defects, which are a main carrier of plastic deformation. They constitute a discontinuity separating a plastically slipped region from unslipped ones, as shown in Fig. 1. A dislocation segment within a crystal is characterized by two vectorial quantities: the tangent vector $\underline{t}$ on the dislocation line and the Burgers vector $\underline{b}$. The latter defines both magnitude and direction of the plastic slip carried by the dislocation. Performing a Burgers circuit around a dislocated crystal domain and comparing it to the same circuit around a perfect crystal domain yields the closure failure due to the dislocation. With respect to some

[1] Under certain conditions, this is not sufficient and more elaborate approaches are necessary [48].

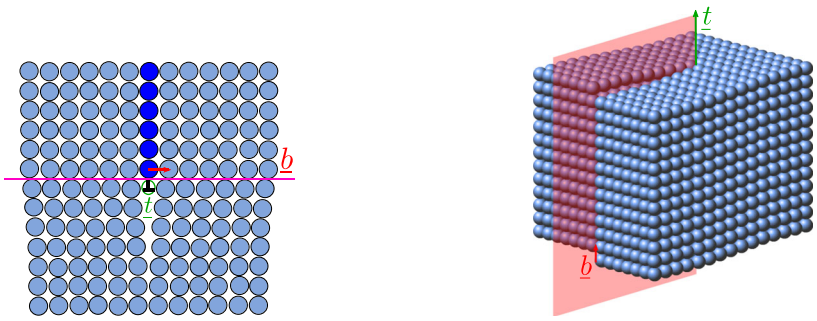

Fig. 1 Edge dislocation with $\underline{b} \perp \underline{t}$ (left) and screw dislocation with $\underline{b} \parallel \underline{t}$ (right, on the basis of www.spaceflight.esa.int/impress/text/education) in a simple cubic lattice

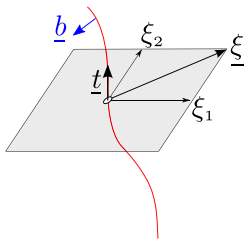

Fig. 2 Single dislocation (red line) characterized by its Burgers vector $\underline{b}$ and local tangent vector $\underline{t}$. The tangent plane (gray) is perpendicular to $\underline{t}$

sign convention, this yields exactly the dislocation's elementary Burgers vector $\underline{b}$.[2] The motion of dislocations is confined to certain crystallographic planes with the normal $\underline{m} \sim \underline{b} \times \underline{t}$. According to Nye, Kröner and Bilby, a single dislocation segment as illustrated in Fig. 2 can be characterized by a second-order dislocation (density) tensor [27]:

$$\underline{\underline{\alpha}} = \underline{b} \otimes \underline{t}\ \delta(\xi_1)\,\delta(\xi_2) = \underline{b} \otimes \underline{t}\ \delta^2(\underline{\xi}). \tag{1}$$

Here, $\delta(\xi_i)$ and $\delta^2(\underline{\xi})$ represent the one- and two-dimensional Dirac delta function, respectively.

As shown in Eq. (1), the tensor of a single dislocation segment contains the dyadic product of its Burgers vector and its tangent vector. Considering N single dislocation lines within a finite crystal volume, the ensemble may be characterized by its mean dislocation density tensor summing up the contributions of each segment with its density ρ_{d}^n:

$$\underline{\underline{\alpha}} = \sum_{n=1}^{N} \rho_{\mathrm{d}}^n\ \underline{b}_n \otimes \underline{t}_n. \tag{2}$$

This equation represents a starting point for suitable averaging techniques performing the transition from discrete dislocations to a continuous distribution [27,47].

2.2 Kinematics of dislocation ensembles

The essential kinematical assumption of geometrically linear continuum dislocation theory is the additive split of the total deformation (the displacement gradient) into an elastic and a plastic part:[3]

$$\mathrm{grad}(\underline{u}) =: \underline{\underline{\beta}} = \underline{\underline{\beta}}_{\mathrm{e}} + \underline{\underline{\beta}}_{\mathrm{p}}. \tag{3}$$

It is typical for the theory that the plastic part is considered a result of the collective motion of continuously distributed dislocations. Dislocations are thus introduced *by their effect*. The *resultant* Burgers vector, i.e., the

[2] In the following, this will be referred to as *elementary* Burgers vector in contrast to the *resultant* Burgers vector of some dislocation ensemble.

[3] Note that upright indices are labels (e.g., p stands for plastic), whereas italic indices $a, b, \ldots$ stand for Cartesian coordinates x, y, z.

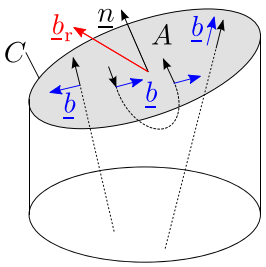

Fig. 3 Resultant Burgers vector $\underline{b}_\mathrm{r}$ of some finite area A with contour $C = \partial A$. Additionally, some exemplary *discrete* dislocations lines leading to $\underline{b}_\mathrm{r}$ are sketched

resulting closure failure, characterizes an *ensemble* of dislocations. As the crystal lattice is not incorporated in the continuum theory, the Burgers circuit (cf. Sect. 2.1) cannot be performed around some ensemble to measure its resultant Burgers vector. As an alternative, the incompatibility of the plastic distortion field indicates the presence of dislocations. Thus, the resulting closure failure can be obtained from a closed-loop path integral over $\underline{\underline{\beta}}_\mathrm{p}$ instead of $\underline{\underline{\beta}}$ [30]:

$$\oint_C \underline{\underline{\beta}} \cdot \mathrm{d}\underline{r} = \underline{0} \quad \text{but} \quad \oint_C \underline{\underline{\beta}}_\mathrm{p} \cdot \mathrm{d}\underline{r} = \int_A \mathrm{curl}\left(\underline{\underline{\beta}}_\mathrm{p}\right) \cdot \underline{n}\, \mathrm{d}A = \underline{b}_\mathrm{r}, \tag{4}$$

where C stands for the contour of the area A. This relation has the consequence of a homogenization: $\underline{b}_\mathrm{r}$ sums up the elementary Burgers vectors of all dislocations piercing the cut face with the unit normal vector $\underline{n}$ and lying within the domain A, as shown in Fig. 3. Contributions from SSDs therefore cancel out (by definition). Hence, $\underline{b}_\mathrm{r}$ is a measure of the number and character of all GNDs piercing this area.

For an infinitesimally small area, the integration may be omitted and the dislocation (density) tensor $\underline{\underline{\alpha}}$ in the continuum theory is identified as [4,30]:

$$\mathrm{d}\underline{b}_\mathrm{r} = \mathrm{curl}(\underline{\underline{\beta}}_\mathrm{p}) \cdot \underline{n}\, \mathrm{d}A \quad \Rightarrow \quad \underline{\underline{\alpha}} := \mathrm{curl}(\underline{\underline{\beta}}_\mathrm{p}). \tag{5}$$

Dividing $\mathrm{d}\underline{b}_\mathrm{r}$ by $\mathrm{d}A$ yields a dislocation vector related to the corresponding tensor with a Cauchy-like formula:

$$\frac{\mathrm{d}\underline{b}_\mathrm{r}}{\mathrm{d}A} = \underline{a}(\underline{r}, \underline{n}) = \underline{\underline{\alpha}} \cdot \underline{n}. \tag{6}$$

In contrast to the resultant Burgers vector, which depends on the integration circuit, the dislocation vector $\underline{a}$ is a *local* quantity. The dislocation tensor carries the information about the dislocation vectors with respect to any cut face with normal $\underline{n}$. Obviously, there is a wide-ranging formal analogy between the stress vector and tensor and the dislocation vector and tensor [52].[4] Dividing the norm of the dislocation vector by the norm of the crystal's elementary Burgers vector ($|\underline{b}| =: b$) yields a measure of the geometrically necessary dislocation density within the cut face with normal $\underline{n}$:

$$\rho_\mathrm{d}(\underline{r}, \underline{n}) = \frac{|\underline{a}(\underline{r}, \underline{n})|}{|\underline{b}|} = \frac{1}{b} \left|\underline{\underline{\alpha}}(\underline{r}) \cdot \underline{n}\right|. \tag{7}$$

Choosing the cut face perpendicular to the slip plane and to the slip direction, ρ_d measures the dislocation density per slip system (for an illustration, see Sect. 6).[5] Another possible definition independent of any cut surface is obtained from the Euclidean norm of the dislocation tensor (cf. "Appendix A"):

$$\rho_\mathrm{d}(\underline{r}) = \frac{1}{b} \|\underline{\underline{\alpha}}\|. \tag{8}$$

For the special case considered in Sect. 5, Definitions (7) and (8) are equivalent. As shown in [51], there are also (principal) invariants of $\underline{\underline{\alpha}}$ that explicitly separate the screw and edge part from each other.

[4] However, in contrast to the stress tensor $\underline{\underline{\sigma}}$ the dislocation tensor $\underline{\underline{\alpha}}$ is *not* symmetric.

[5] In Eq. (7) ρ_d represents the number of dislocations piercing (locally) the cut face, which is in general not equal to the competing definition as total dislocation line length per volume [3].

3 Kinetics of a continuously dislocated crystal from energetic principles

In this section, field equations are derived by the aid of energetic principles. Therefore, it is assumed that the state of the continuously dislocated crystal is well defined by a set of state variables. Consequently, the (free) energy of the system is a state function.

3.1 Free energy of a continuously dislocated crystal

The state of a crystal with continuously distributed dislocations is assumed to depend solely on the elastic strain $\underline{\underline{\varepsilon}}_{\mathrm{e}} = \operatorname{sym}(\underline{\underline{\beta}}_{\mathrm{e}})$, on the dislocation density tensor $\underline{\underline{\alpha}} = \operatorname{curl}(\underline{\underline{\beta}}_{\mathrm{p}})$ and on the thermodynamic temperature θ [4,30]. Accordingly, the free-energy density only depends on these three thermodynamical state variables. The following additive decomposition is assumed:

$$\phi = \phi(\theta, \underline{\underline{\varepsilon}}_{\mathrm{e}}, \underline{\underline{\alpha}}) = \phi_{\mathrm{t}}(\theta) + \phi_{\mathrm{e}}(\underline{\underline{\varepsilon}}_{\mathrm{e}}) + \phi_{\mathrm{p}}(\underline{\underline{\alpha}}). \tag{9}$$

The thermal part $\phi_{\mathrm{t}}(\theta)$ shall not be further concretized since the heat conduction problem is not considered in this study. The elasticity of the crystal contributes to the total free-energy twofold: The part ϕ_{e} represents the macroscopic strain energy and takes the form known from linear elasticity theory:

$$\phi_{\mathrm{e}}(\underline{\underline{\varepsilon}}_{\mathrm{e}}) = \mu \|\underline{\underline{\varepsilon}}_{\mathrm{e}}\|^2 + \tfrac{1}{2}\lambda(\underline{\underline{I}} \cdot\cdot\, \underline{\underline{\varepsilon}}_{\mathrm{e}})^2 \tag{10}$$

with Lamé's constants μ and λ.[6] The part ϕ_{p} arises from the microscopic elastic energy due to the dislocation network and is assumed as

$$\phi_{\mathrm{p}}(\underline{\underline{\alpha}}) = k\mu \ln\left[\left(1 - \frac{\rho_{\mathrm{d}}}{\rho_{\mathrm{s}}}\right)^{-1}\right] \quad \text{with} \quad \rho_{\mathrm{d}} = \frac{1}{b}\|\underline{\underline{\alpha}}\|. \tag{11}$$

Here, k is a dimensionless weighting factor and ρ_{s} represents the saturation value of the dislocation density. Characterizing the closest admissible packing of dislocations in a discrete crystal lattice, ρ_{s} is a well-defined physical quantity.[7] The logarithmic term ensures a linear increase of the energy for small dislocation density ρ_{d} and tends to infinity as ρ_{d} approaches ρ_{s} [6]. This provides an energetic barrier against over-saturation (see also the reasoning based on statistical mechanics of dislocations in [4,5]). Overall, there are only five material parameters $\mu, \lambda, b, k, \rho_{\mathrm{s}}$ describing the mechanical part of the free energy stored within the material.

3.2 Field equations and boundary conditions from minimizing the potential energy

At this stage of the theory, it is already possible to obtain governing field equations by minimizing the total potential energy of the system. Besides the temperature field (not considered here), there are two other primary fields in geometric linear CDT: the displacement $\underline{u}$ and the plastic distortion $\underline{\underline{\beta}}_{\mathrm{p}}$. From them, thermodynamic state variables are derived [cf. Eqs. (3) and (5)]:

$$\underline{\underline{\varepsilon}}_{\mathrm{e}} = \operatorname{sym}(\operatorname{grad}(\underline{u}) - \underline{\underline{\beta}}_{\mathrm{p}}), \tag{12}$$

$$\underline{\underline{\alpha}} = -\operatorname{curl}(\operatorname{grad}(\underline{u}) - \underline{\underline{\beta}}_{\mathrm{p}}) = \operatorname{curl}(\underline{\underline{\beta}}_{\mathrm{p}}). \tag{13}$$

The total internal potential energy is obtained by integrating the free-energy density over the volume V of the body:

$$\Pi_{\mathrm{in}} = \int_V \phi \,\mathrm{d}V = \int_V \phi_{\mathrm{e}}\left(\operatorname{sym}(\underline{\underline{\beta}} - \underline{\underline{\beta}}_{\mathrm{p}})\right) + \phi_{\mathrm{d}}\left(\operatorname{curl}(\underline{\underline{\beta}}_{\mathrm{p}})\right) \mathrm{d}V. \tag{14}$$

[6] For the sake of compact analytical expressions (cf. Sect. 5), *isotropic* elasticity is assumed. Of course, most real single crystals exhibit *anisotropic* elastic behavior.

[7] For this reason, the saturation density is not an arbitrary scaling parameter which has to drop out of the constitutive equations [22], cf. also [19].

The total external potential energy should include all kinematically relevant processes [20] and has thus several contributions. As there are two independent primary fields, the existence of two corresponding external surface loads is assumed: The stress vector $\underline{s}$ drives the displacement $\underline{u}(\underline{r})$ of the body and $\underline{\underline{S}}$ drives the plastic distortion $\underline{\underline{\beta}}_{\mathrm{p}}(\underline{r})$, i.e., the collective motion of dislocations.[8] Additionally, mass forces due to external fields $\underline{f}$ are considered as well. Altogether, this provides

$$\Pi_{\mathrm{ex}} = -\int_V \rho\, \underline{f} \cdot \underline{u}\, \mathrm{d}V - \int_{\partial V} \underline{s} \cdot \underline{u}\, \mathrm{d}A - \int_{\partial V} \underline{\underline{S}} \cdot\cdot\, \underline{\underline{\beta}}_{\mathrm{p}}^{\mathrm{T}}\, \mathrm{d}A, \tag{15}$$

where V is the volume of the material body and ∂V denotes its surface. The sum of both contributions Π_{in} and Π_{ex} yields the total potential energy. In order to minimize it, the first variation has to vanish, i.e., $\delta\Pi_{\mathrm{in}} + \delta\Pi_{\mathrm{ex}} = 0$:

$$\begin{aligned} &\int_V \left(\frac{\delta\phi}{\delta \underline{u}} - \rho\, \underline{f} \right) \cdot \delta \underline{u}\, \mathrm{d}V + \int_V \frac{\delta\phi}{\delta \underline{\underline{\beta}}_{\mathrm{p}}} \cdot\cdot\, \delta \underline{\underline{\beta}}_{\mathrm{p}}^{\mathrm{T}}\, \mathrm{d}V \\ &+ \int_{\partial V} \left(\frac{\partial\phi}{\partial \underline{\underline{\beta}}} \cdot \underline{n} - \underline{s} \right) \cdot \delta \underline{u}\, \mathrm{d}A + \int_{\partial V} \left(-\frac{\partial\phi}{\partial \underline{\underline{\alpha}}} \cdot \underline{\underline{\epsilon}} \cdot \underline{n} - \underline{\underline{S}} \right) \cdot\cdot\, \delta \underline{\underline{\beta}}_{\mathrm{p}}^{\mathrm{T}}\, \mathrm{d}A = 0. \end{aligned} \tag{16}$$

Here, $\underline{n}$ is a unit outward normal and $\underline{\underline{\epsilon}}$ denotes the antisymmetric isotropic tensor of third order (a.k.a Ricci permutation tensor), which has the following property:

$$\underline{v} \cdot \underline{\underline{\epsilon}}^{\mathrm{T}} \cdot \underline{w} = -\underline{v} \cdot \underline{\underline{\epsilon}} \cdot \underline{w} = \underline{v} \times \underline{w}. \tag{17}$$

Mathematically speaking Eq. (16) is the *weak* form of the problem. Exploiting the fundamental law of the calculus of variation, two classes of equations can be deduced: Considering the volume integrals appearing in Eq. (16), we obtain the Euler equations

$$\frac{\delta\phi}{\delta \underline{u}} = \rho\, \underline{f} \quad \rightarrow \quad \frac{\partial\phi}{\partial \underline{u}} - \mathrm{div} \left(\frac{\partial\phi}{\partial \underline{\underline{\beta}}} \right) = \rho\, \underline{f}, \tag{18a}$$

$$\frac{\delta\phi}{\delta \underline{\underline{\beta}}_{\mathrm{p}}} = \underline{\underline{0}} \quad \rightarrow \quad \frac{\partial\phi}{\partial \underline{\underline{\beta}}_{\mathrm{p}}} + \mathrm{curl} \left(\frac{\partial\phi}{\partial \underline{\underline{\alpha}}} \right) = \underline{\underline{0}}. \tag{18b}$$

Considering the surface integrals of the weak form (16) reveals the natural boundary conditions of the problem:

$$\frac{\partial\phi}{\partial \underline{\underline{\beta}}} \cdot \underline{n} = \underline{s}, \quad \frac{\partial\phi}{\partial \underline{\underline{\alpha}}} \times \underline{n} = \underline{\underline{S}}. \tag{19}$$

The conditions for free boundaries are obtained immediately setting the right-hand side of Eq. (19) zero. This is discussed in more detail in Sect. 5.3. Euler Equations (18) together with the boundary conditions (19) represent the *strong* form of the problem. In the following sections, it will be shown that the minimization of the total potential energy is compatible with the constitutive equations for the case of zero dissipation (cf. Sect. 4.4.1).

3.3 Field equations from the phase field method

Another possible means of deriving field equations for the geometric linear CDT is the phase field method (PFM), cf., e.g., [8,16,29,41]. One branch of the PFM—the continuum diffusive-interface approach—treats the interface between two phases as a region of finite width having a *gradual* variation of physical quantities [16]. In order to distinguish one phase from the other, auxiliary primary variables, the phase fields, are introduced. If they are not conserved—which is the only case considered here—relaxational or Ginzburg–Landau type field

[8] The existence of $\underline{\underline{S}}$ is necessary to retain the method of sections: The effect of the cutoff part is captured by the $\underline{\underline{S}}$-field on the cut surface.

equations are obtained [8]: Given the free energy density of a system as a function of some primary (phase) field variables $f_i(\underline{r})$ and their gradients $\underline{\nabla} f_i(\underline{r})$:

$$\phi\Big(f_1(\underline{r}),\, f_2(\underline{r}),\, \underline{\nabla} f_1(\underline{r}),\, \underline{\nabla} f_2(\underline{r}),\, \dots\Big)$$

the evolution of *non-conserved* phase fields f_i is assumed in the following way.[9] The rate of the primary fields is set proportionally to the negative variational derivatives of the total free energy with respect to the corresponding primary field:

$$\dot{f}_i = -\frac{1}{\eta_i}\frac{\delta\phi}{\delta f_i}, \tag{20}$$

with η_i being some damping constant or, equivalently, $1/\eta_i$ representing the relaxation rate. Equation (20) is called Ginzburg–Landau equation. With the considerations from Sect. 3.2, it is clear that this approach drives the system toward the energy minimum. Changing the phase field in the direction of $-\delta\phi/\delta f_i$ is guaranteed to reduce ϕ till a minimum is reached [8]. In many applications in physics and materials science, this is a reasonable assumption (if nothing else is known about the dynamics of the system). In the case of the geometrically linear CDT, this approach yields:

$$\dot{\underline{u}} = -\frac{1}{\eta_\mathrm{u}}\frac{\delta\phi}{\delta\underline{u}}, \quad \dot{\underline{\underline{\beta}}}_\mathrm{p} = -\frac{1}{\eta_\mathrm{p}}\frac{\delta\phi}{\delta\underline{\underline{\beta}}_\mathrm{p}}. \tag{21}$$

In contrast to Sect. 3.2, this is a *dynamical* formulation of the theory.[10] Not only the initial and the final state of the system can be calculated, but also the temporal evolution between those states. In the context of CDT, it is obvious that the plastic distortion $\underline{\underline{\beta}}_\mathrm{p}$ distinguishes the *elastic* "phase" from the *plastic* one by a smooth transition. To be precise, one should speak of *merely elastically deformed* regions and *plastically slipped* regions of the body. Furthermore, the dislocation network energy plays the role of the well-known gradient energy of the PFM. More examples of the application of the ideas presented in this section are given in [24,41]. At this point, it becomes important to investigate the thermodynamical consequences of such modeling.

4 Thermodynamics of a continuously dislocated crystal

As will be seen now, the derived field equations of Sect. 3 can be found as special cases of a more rigorous thermodynamical consideration. This will allow studying the physical consequences of some previous assumptions and proving the thermodynamical consistency of the theory.[11]

4.1 Internal and external mechanical power

Given a material body B with the total mass M, the total volume V and a surface A (with $A = \partial V$), the external forces acting on the body are now defined. As argued in Sect. 3.2, the existence of two external surface loads is assumed: The stress vector $\underline{s}$ drives the displacement $\underline{u}(\underline{r})$ of the body and $\underline{\underline{S}}$ drives the plastic distortion $\underline{\underline{\beta}}_\mathrm{p}(\underline{r})$, i.e., the collective motion of dislocations. Additionally, mass forces due to external fields $\underline{f}$ are considered as well. Hence, the external mechanical power takes the form:

$$P_\mathrm{ex} = \int_A \dot{\underline{u}} \cdot \underline{s}\, \mathrm{d}A + \int_M \dot{\underline{u}} \cdot \underline{f}\, \mathrm{d}m + \int_A \dot{\underline{\underline{\beta}}}_\mathrm{p}^\mathrm{T} \cdot\cdot\, \underline{\underline{S}}\, \mathrm{d}A. \tag{22}$$

[9] The fields $f_i(\underline{r})$ can be tensors of different orders.

[10] This theory is coarser-grained than [56] since not the individual dislocations are treated as phase field objects but only the geometric effect of incompatibility caused by dislocation ensembles.

[11] An even more general thermodynamic framework including the presented approach as a special case was developed in [54].

The kinetic energy of the system is assumed to solely depend on the velocity, i.e., the material time derivative of $\underline{u}(\underline{r})$:

$$E_{\mathrm{kin}} = \frac{1}{2}\int_M \dot{\underline{u}}\cdot\dot{\underline{u}}\,\mathrm{d}m, \quad \dot{E}_{\mathrm{kin}} = \int_M \dot{\underline{u}}\cdot\ddot{\underline{u}}\,\mathrm{d}m. \tag{23}$$

Subtracting the rate of the kinetic energy from the external mechanical power yields the internal mechanical power:

$$P_{\mathrm{in}} = P_{\mathrm{ex}} - \dot{E}_{\mathrm{kin}} = \int_A \dot{\underline{u}}\cdot\underline{s}\,\mathrm{d}A + \int_M \dot{\underline{u}}\cdot\underline{f}\,\mathrm{d}m + \int_A \dot{\underline{\underline{\beta}}}_{\mathrm{p}}^{\mathrm{T}} \cdot\cdot\, \underline{\underline{S}}\,\mathrm{d}A - \int_M \dot{\underline{u}}\cdot\ddot{\underline{u}}\,\mathrm{d}m.$$

Now, Cauchy's formula is exploited and a similar relation between the kinetic quantity $\underline{\underline{S}}$, which is power-conjugate to $\dot{\underline{\underline{\beta}}}_{\mathrm{p}}$, and a higher-order stress tensor $\underline{\underline{\underline{\Sigma}}}$ is assumed [33]:

$$\underline{s} = \underline{\underline{\sigma}}\cdot\underline{n}, \quad \underline{\underline{S}} = \underline{\underline{\underline{\Sigma}}}\cdot\underline{n}. \tag{24}$$

The energetical contribution $\phi_{\mathrm{p}}(\underline{\underline{\alpha}})$ (11) leads necessarily to the existence of higher-order stresses [1,32], which are related to the eigenstrain field of dislocations or ensembles of them and thus have a clear physical meaning (cf. also Sects. 5.2 and 5.3). Hence, the total internal power can be written as

$$P_{\mathrm{in}} = \int_A (\dot{\underline{u}}\cdot\underline{\underline{\sigma}} + \dot{\underline{\underline{\beta}}}_{\mathrm{p}}^{\mathrm{T}} \cdot\cdot\, \underline{\underline{\underline{\Sigma}}})\cdot\underline{n}\,\mathrm{d}A + \int_M \dot{\underline{u}}\cdot(\underline{f} - \ddot{\underline{u}})\,\mathrm{d}m. \tag{25}$$

Using Gauss' theorem (cf. "Appendix A") allows transformation of the surface integral into a volume integral and finally identifying the internal power density p_{in}:

$$P_{\mathrm{in}} = \int_V \Big(\mathrm{div}(\dot{\underline{u}}\cdot\underline{\underline{\sigma}}) + \mathrm{div}(\dot{\underline{\underline{\beta}}}_{\mathrm{p}}^{\mathrm{T}} \cdot\cdot\, \underline{\underline{\underline{\Sigma}}}) + \dot{\underline{u}}\cdot\rho(\underline{f} - \ddot{\underline{u}})\Big)\,\mathrm{d}V = \int_V p_{\mathrm{in}}\,\mathrm{d}V. \tag{26}$$

4.2 Evaluation of the second law of thermodynamics

As a starting point consider the mechanical part of the Clausius–Duhem inequality, i.e., the Clausius–Planck inequality:[12]

$$\text{Dissipation} = p_{\mathrm{in}} - (\dot{\phi} + \dot{\theta}s) \geq 0 \quad \text{with} \quad s =: -\frac{\partial\phi}{\partial\theta}, \tag{27}$$

with the free-energy density ϕ and the entropy density s. The various assumptions leading to this inequality (cf., e.g., [44]) are all compatible with CDT. Taking the material time derivative of the free energy $\phi(\underline{\underline{\varepsilon}}_{\mathrm{e}}, \underline{\underline{\alpha}}, \theta)$ given by (9), Inequality (27) becomes

$$p_{\mathrm{in}} - \left(\frac{\partial\phi}{\partial\underline{\underline{\varepsilon}}_{\mathrm{e}}} \cdot\cdot\, \dot{\underline{\underline{\varepsilon}}}_{\mathrm{e}}^{\mathrm{T}} + \frac{\partial\phi}{\partial\underline{\underline{\alpha}}} \cdot\cdot\, \dot{\underline{\underline{\alpha}}}^{\mathrm{T}} + \frac{\partial\phi}{\partial\theta}\dot{\theta} + \dot{\theta}s\right) \geq 0. \tag{28}$$

By Definition $(27)_2$, the last two terms in Inequality (28) cancel out. Inserting Relation (26) for the internal power p_{in} and using some tensor analysis (cf. "Appendix A") finally yields [33]:

$$\begin{aligned}&\Big(\mathrm{div}(\underline{\underline{\sigma}}) + \rho(\underline{f} - \ddot{\underline{u}})\Big)\cdot\dot{\underline{u}} + \left(\underline{\underline{\sigma}} - \frac{\partial\phi}{\partial\underline{\underline{\beta}}}\right) \cdot\cdot\, \mathrm{grad}(\dot{\underline{u}})^{\mathrm{T}} \\ &+ \left(\mathrm{div}\left(\underline{\underline{\underline{\Sigma}}}\right) - \frac{\partial\phi}{\partial\underline{\underline{\beta}}_{\mathrm{p}}}\right) \cdot\cdot\, \dot{\underline{\underline{\beta}}}_{\mathrm{p}}^{\mathrm{T}} + \left(\underline{\underline{\underline{\Sigma}}} - \frac{\partial\phi}{\partial\underline{\underline{\alpha}}}\cdot\underline{\underline{\epsilon}}^{\mathrm{T}}\right) \cdots \mathrm{grad}(\dot{\underline{\underline{\beta}}}_{\mathrm{p}})^{\mathrm{T}} \geq 0.\end{aligned} \tag{29}$$

[12] Since the heat conduction problem is not considered in this study, the pure thermal part of the Clausius–Duhem inequality can be ignored.

Introducing the following abbreviations for the thermodynamic forces, which have appeared naturally [33],

$$\underline{t} \coloneqq \operatorname{div}(\underline{\underline{\sigma}}) + \rho(\underline{f} - \underline{\ddot{u}}), \qquad \underline{\underline{\tau}} \coloneqq \underline{\underline{\sigma}} - \frac{\partial \phi}{\partial \underline{\underline{\beta}}} \quad , \tag{30a}$$

$$\underline{\underline{\kappa}} \coloneqq \operatorname{div}(\underline{\underline{\underline{\Sigma}}}) - \frac{\partial \phi}{\partial \underline{\underline{\beta}}_{\mathrm{p}}} \quad , \qquad \underline{\underline{\underline{T}}} \coloneqq \underline{\underline{\underline{\Sigma}}} - \frac{\partial \phi}{\partial \underline{\alpha}} \cdot \underline{\underline{\epsilon}}^{\mathrm{T}}. \tag{30b}$$

yields at a compact form of the Clausius–Planck inequality for geometric linear continuum dislocation theory:

$$\underline{t} \cdot \dot{\underline{u}} + \underline{\underline{\tau}} \cdot\cdot \operatorname{grad}(\dot{\underline{u}})^{\mathrm{T}} + \underline{\underline{\kappa}} \cdot\cdot \dot{\underline{\underline{\beta}}}_{\mathrm{p}}^{\mathrm{T}} + \underline{\underline{\underline{T}}} \cdots \operatorname{grad}(\dot{\underline{\underline{\beta}}}_{\mathrm{p}})^{\mathrm{T}} \geq 0. \tag{31}$$

The quantities $\underline{\underline{\tau}}$, $\underline{\underline{\kappa}}$ and $\underline{\underline{\underline{T}}}$ all reflect the deviation from potential relations and thus have the meaning of dissipative thermodynamic forces. Furthermore, the material time derivatives of kinematic quantities appear as conjugated thermodynamic fluxes $\dot{\underline{u}}$, $\dot{\underline{\underline{\beta}}} = \operatorname{grad}(\dot{\underline{u}})$, $\dot{\underline{\underline{\beta}}}_{\mathrm{p}}$ and $\operatorname{grad}(\dot{\underline{\underline{\beta}}}_{\mathrm{p}})$.[13]

At this point, several procedures are possible. The relations between thermodynamic forces and fluxes can be chosen directly in such a way that Inequality (31) is fulfilled. This leads to *one specific* set of constitutive equations. Another procedure which leaves the constitutive relations open to a certain degree is obtained by the introduction of a dissipation potential

$$\mathscr{d} = \mathscr{d}_{\mathrm{ex}}(\dot{\underline{u}}) + \mathscr{d}_{\mathrm{in}}(\dot{\underline{\underline{\beta}}}, \dot{\underline{\underline{\beta}}}_{\mathrm{p}}, \operatorname{grad} \dot{\underline{\underline{\beta}}}_{\mathrm{p}}) \tag{32}$$

and a dimensionless constant Λ such that following potential relations hold:

$$\underline{t} \coloneqq \Lambda \frac{\partial \mathscr{d}}{\partial \dot{\underline{u}}}, \quad \underline{\underline{\tau}} \coloneqq \Lambda \frac{\partial \mathscr{d}}{\partial \dot{\underline{\underline{\beta}}}}, \quad \underline{\underline{\kappa}} \coloneqq \Lambda \frac{\partial \mathscr{d}}{\partial \dot{\underline{\underline{\beta}}}_{\mathrm{p}}}, \quad \underline{\underline{\underline{T}}} \coloneqq \Lambda \frac{\partial \mathscr{d}}{\partial \operatorname{grad} \dot{\underline{\underline{\beta}}}_{\mathrm{p}}}. \tag{33}$$

Here, an additive split of the dissipation potential $\mathscr{d}$ was postulated: $\mathscr{d}_{\mathrm{ex}}$ represents external sources of dissipation and $\mathscr{d}_{\mathrm{in}}$ stands for dissipative processes within the material. Further restrictions on the form of $\mathscr{d}$ then ensure the fulfillment of the restriction (31), which will be discussed in Sect. 4.3. Prior to that, some remarks are necessary with regard to general physical aspects of the theory.

Remark 1 For the sake of Galilean invariance, the dissipation must not depend on the velocity $\dot{\underline{u}}$ and hence $\mathscr{d}_{\mathrm{ex}} = 0$. It then follows $\underline{t} = \operatorname{div}(\underline{\underline{\sigma}}) + \rho(\underline{f} - \underline{\ddot{u}}) = \underline{0}$. This is the well-known local balance of momentum from standard continuum mechanics. This aspect will be further addressed in Sects. 4.4.1 and 4.4.2.

Remark 2 The first law of thermodynamics predicts a change of temperature if there is dissipation. In other words, *dissipative processes cannot be isothermal*: The dissipated energy is transformed into internal energy. Consequently, the heat conduction problem must be addressed in future studies.

Remark 3 In the derivation of Inequality (27), it is assumed that the entropy flux is solely given by the heat flux divided by the absolute temperature. The heat flux again is a function of temperature as well. The temperature in continuum physics represents microscopical degrees of freedom (motion of atoms or molecules). Exactly the same applies to the plastic distortion $\underline{\underline{\beta}}_{\mathrm{p}}$: It represents the degrees of freedom of (continuously distributed) dislocations. Hence, not only entropy production (dissipation) by dislocation movement, as assumed above, is imaginable, but also a corresponding entropy flux (cf. [16]).

4.3 Physical interpretation of the dissipation potential

There are innumerable possibilities to fulfill the Clausius–Planck inequality in the Form (31). Here, a particularly meaningful restriction on the choice of constitutive relations is presented.

Let $\overset{\circ}{a}_i$ denote any thermodynamic flux and let $\{\overset{\circ}{a}_i\}$ stand for a set of fluxes. Further, $\mathscr{d}(\overset{\circ}{a}_i)$ is assumed as a homogeneous function of degree n, i.e., for any constant c holds $\mathscr{d}(c\ \overset{\circ}{a}_i) = c^n \mathscr{d}(\overset{\circ}{a}_i)$. Now a well-known Euler theorem states

$$\sum_i \overset{\circ}{a}_i \cdot \frac{\partial \mathscr{d}(\{\overset{\circ}{a}_i\})}{\partial \overset{\circ}{a}_i} = n\ \mathscr{d}(\{\overset{\circ}{a}_i\}), \quad \text{here}: \quad \{\overset{\circ}{a}_i\} = \dot{\underline{u}}, \dot{\underline{\underline{\beta}}}, \dot{\underline{\underline{\beta}}}_{\mathrm{p}}, \operatorname{grad} \dot{\underline{\underline{\beta}}}_{\mathrm{p}}. \tag{34}$$

[13] Note that the choice of thermodynamic fluxes and forces is not unique.

Further assuming $n > 0$ and $\mathscr{d}(\overset{\circ}{a}_i) > 0 \; \forall \; \overset{\circ}{a}_i$, Inequality (31) is fulfilled *a priori* by adopting Potential Relations (33). Moreover, choosing $\Lambda = 1/n$ yields the identity of the dissipation potential and the dissipated power itself. Thus, a direct physical interpretation of $\mathscr{d}$ is gained. In other words, the procedure represents a physically based reduction of options for the relations between thermodynamic forces and fluxes. Another, but more restrictive, possibility for guaranteeing inequality (31) is the assumption of $\mathscr{d}(\overset{\circ}{a}_i)$ being a positive and convex function.

4.4 Different dissipation mechanisms

Depending on the set of independent variables of $\mathscr{d}$, different general material models within CDT can be deduced depending on the dissipative mechanisms considered. In this section, a wide range of such mechanisms is presented.

4.4.1 Elastic–plastic behavior without dissipation

In the case of no dissipation at all, $\underline{t} = \underline{0}$, $\underline{\tau} = \underline{0}$, $\underline{\kappa} = \underline{0}$, $\underline{\underline{T}} = \underline{\underline{0}}$ hold. Then Relations (33) with Definitions (30) lead to

$$\operatorname{div}(\underline{\sigma}) + \rho(\underline{f} - \ddot{\underline{u}}) = \underline{0}\,, \quad \underline{\sigma} = \frac{\partial \phi}{\partial \underline{\beta}}\,, \quad \operatorname{div}(\underline{\underline{\Sigma}}) = \frac{\partial \phi}{\partial \underline{\beta}_{\mathrm{p}}}\,, \quad \underline{\underline{\Sigma}} = -\frac{\partial \phi}{\partial \underline{\alpha}} \cdot \underline{\underline{\epsilon}}. \tag{35}$$

Equation $(35)_1$ is the well-known local force balance. The second equation is the potential relation for the stress tensor known from linear elasticity theory. Inserting Eq. $(35)_2$ into $(35)_1$ and Eq. $(35)_4$ into $(35)_3$ yields the partial differential equations for the primary variables:

$$\operatorname{div}\left(\frac{\partial \phi}{\partial \underline{\beta}}\right) = \rho(\ddot{\underline{u}} - \underline{f}), \quad \frac{\partial \phi}{\partial \underline{\beta}_{\mathrm{p}}} + \operatorname{curl}\left(\frac{\partial \phi}{\partial \underline{\alpha}}\right) = \underline{\underline{0}}. \tag{36}$$

Note that these constitutive relations are identical to Eq. (18) which were found by minimizing the total potential energy of the system.[14] This behavior could also be called pseudo-elastic in the sense that there is no dissipation. However, the plastic distortion is not reversible and the body does not regain its initial configuration after unloading.

The interpretation of this result is of great importance: Plastic distortion is possible even though all external work done on the body is saved as strain energy and dislocation network energy. In the special case of a deformation process with boundary conditions allowing the total deformation to be only plastic and homogeneous, no energy is saved within the material. Hence, no external work is necessary and there is a zero-energy deformation mode, which is unphysical. Consequently, it is essential to consider the dissipative character of dislocation motion.

4.4.2 Damped elastic behavior

If the dissipation depends solely on velocity $\dot{\underline{u}}$, i.e., $\mathscr{d} = \mathscr{d}_{\mathrm{ex}}(\dot{\underline{u}})$, the displacement of all material particles is damped with respect to their velocity. Assuming this form of the dissipation potential yields a dynamic theory with some damping forces acting on all material points. The local force balance is then

$$\operatorname{div}(\underline{\sigma}) + \rho(\underline{f} - \ddot{\underline{u}}) = \Lambda \frac{\partial \mathscr{d}_{\mathrm{ex}}}{\partial \dot{\underline{u}}}. \tag{37}$$

As an example, assume a simple quadratic form of the external dissipation potential $\mathscr{d}_{\mathrm{ex}} = \eta_{\mathrm{u}} \dot{\underline{u}} \cdot \dot{\underline{u}}$ and set $\Lambda = 1/2$ according to Sect. 4.3. This results in

$$\rho \ddot{\underline{u}} + \eta_{\mathrm{u}} \dot{\underline{u}} = \operatorname{div}(\underline{\sigma}) + \rho \underline{f} \quad \text{with} \quad \underline{\sigma} = \frac{\partial \phi}{\partial \underline{\beta}}. \tag{38}$$

[14] Using the more general principle of least action, it is possible to also include the inertia forces in Eq. (18).

Evaluating the potential relationship of the stress tensor for ϕ given by Eq. (10) finally yields a hyperbolic partial differential equation for displacement field $\underline{u}(\underline{r}, t)$. Even though the external damping might be questioned from the physical point of view, it is very helpful from the numerical point of view: In the case of a quasi-static deformation one can neglect any inertia forces. However, it is useful to retain the damping forces because the parabolic form

$$\eta_{\mathrm{u}}\dot{\underline{u}} = \operatorname{div}\left(\underline{\underline{\sigma}}(\operatorname{grad}(\underline{u}))\right) + \rho\,\underline{f} \tag{39}$$

is very suitable for developing an explicit solution scheme for the partial differential equation (cf. Sect. 6.2). In fact, Eq. (39) is the over-damped equation of motion of the particle. Thus, the theory can predict the temporal evolution of the system from some initial configuration to the current configuration but without vibrations. This method is also known as dynamic relaxation [57], where the damping constant is chosen in such a way that the system converges to the static solution as quickly as possible. If no other fields $\underline{f}$ are involved, phase field Eq. $(21)_1$ is obtained since

$$\eta_{\mathrm{u}}\dot{\underline{u}} = \operatorname{div}(\underline{\underline{\sigma}}) \equiv -\frac{\delta\phi}{\delta\underline{u}}. \tag{40}$$

This can be proved by calculating the variational derivative of ϕ from Eq. (10) with respect to $\underline{u}$. Consequently, these assumptions lead to the phase field equations from which it is known that the evolution of the field tends toward the energy minimum. Thus, the thermodynamical consistency of phase field Eq. $(21)_1$ is proved as well.

Nevertheless, the proposed approach has one important drawback, which becomes evident from Remarks 1 and 2: Dissipation, i.e., the production of entropy, causes heating of the system. If $\mathscr{d} = \mathscr{d}_{\mathrm{ex}}(\dot{\underline{u}})$, a rigid body motion could cause local heat generation due to the damping forces. This is, of course, not the case. Hence, care must be taken that the damping forces remain sufficiently small. Beyond that, here is a simple remedy for the problem: Let us reject the dependence of the dissipation potential from the local velocity, i.e., $\mathscr{d}_{\mathrm{ex}}(\dot{\underline{u}}) = 0$ and instead define some external force field $\rho\,\underline{f} = -\eta_{\mathrm{u}}\dot{\underline{u}}$. Inserting this into Eq. (37) and neglecting inertia forces, Eq. (40) is obtained *without* the aforementioned drawback. In a sense, the damping effect is thus simply moved outside the thermodynamical system and does not contribute to its dissipation.

4.4.3 Viscoelastic–plastic behavior

If the dissipation solely depends on the velocity gradient $\dot{\underline{\underline{\beta}}} = (\underline{u}\otimes\underline{\nabla})^{\cdot} = (\underline{v}\otimes\underline{\nabla})$, i.e., $\mathscr{d} = \mathscr{d}(\dot{\underline{\underline{\beta}}})$, viscoelastic behavior is obtained. By Eq. (33), $\underline{t} = \underline{0}$, $\underline{\underline{\kappa}} = \underline{\underline{0}}$, $\underline{\underline{\underline{T}}} = \underline{\underline{0}}$ as in Sect. 4.4.1, but

$$\underline{\underline{\tau}} = \left(\underline{\underline{\sigma}} - \frac{\partial\phi}{\partial\underline{\underline{\beta}}}\right) = \Lambda\frac{\partial\mathscr{d}}{\partial\dot{\underline{\underline{\beta}}}}. \tag{41}$$

Re-arranging Eq. (41) suggests that $\underline{\underline{\tau}}$ has the meaning of a viscous contribution to the stress tensor as known from the Newtonian fluid in rheology:

$$\underline{\underline{\sigma}} = \frac{\partial\phi}{\partial\underline{\underline{\beta}}} + \Lambda\frac{\partial\mathscr{d}}{\partial\dot{\underline{\underline{\beta}}}} = \frac{\partial\phi}{\partial\underline{\underline{\beta}}} + \underline{\underline{\tau}}. \tag{42}$$

Furthermore, it becomes obvious that the dissipation should only depend on the symmetric part of the velocity gradient. Otherwise, $\underline{\underline{\tau}}$ would be unsymmetric and the dissipation would depend on the rotational velocity (spin) of the body. As this dissipation mechanism is in general not important for metallic crystals with a small elastic regime, it is not further considered in this study.

4.4.4 Elastic–viscoplastic behavior with local dissipation

If the dissipation depends solely on the rate of plastic distortion, $\mathscr{d} = \mathscr{d}(\dot{\underline{\underline{\beta}}}_{\mathrm{p}})$, elastic-(visco)plastic behavior is obtained. By Eq. (33) $\underline{t} = \underline{0}$, $\underline{\underline{\tau}} = \underline{\underline{0}}$ but

$$\underline{\underline{\kappa}} = \left(\underline{\underline{\underline{\Sigma}}}\cdot\underline{\nabla} - \frac{\partial\phi}{\partial\underline{\underline{\beta}}_{\mathrm{p}}}\right) = \Lambda\frac{\partial\mathscr{d}}{\partial\dot{\underline{\underline{\beta}}}_{\mathrm{p}}} \quad , \quad \underline{\underline{\underline{T}}} = \left(\underline{\underline{\underline{\Sigma}}} + \frac{\partial\phi}{\partial\underline{\underline{\alpha}}}\cdot\underline{\underline{\underline{\epsilon}}}\right) = \underline{\underline{0}}. \tag{43}$$

Inserting relation $(43)_2$ into $(43)_1$ yields a partial differential equation for the primary variable $\underline{\underline{\beta}}_\mathrm{p}$:

$$-\left(\frac{\partial\phi}{\partial\underline{\underline{\beta}}_\mathrm{p}}-\frac{\partial\phi}{\partial\underline{\underline{\alpha}}}\times\underline{\nabla}\right)=\Lambda\frac{\partial\mathscr{d}}{\partial\dot{\underline{\underline{\beta}}}_\mathrm{p}}. \tag{44}$$

Identifying the term on the left-hand side as the negative variational derivative (cf. Sect. 3.2) reveals the well-known Biot-type differential equation [7]:

$$-\frac{\delta\phi}{\delta\underline{\underline{\beta}}_\mathrm{p}}=\Lambda\frac{\partial\mathscr{d}}{\partial\dot{\underline{\underline{\beta}}}_\mathrm{p}}. \tag{45}$$

Depending on the choice of $\mathscr{d}(\dot{\underline{\underline{\beta}}}_\mathrm{p})$, rate-dependent (i.e., viscoplastic) and rate-independent plastic behavior is possible. Examples will be given in Sect. 5.

4.4.5 Elastic–viscoplastic behavior with non-local dissipation

If the dissipation depends on the rate of plastic distortion and its gradient, $\mathscr{d}=\mathscr{d}(\dot{\underline{\underline{\beta}}}_\mathrm{p},\operatorname{grad}\dot{\underline{\underline{\beta}}}_\mathrm{p})$, elastic–(visco)plastic behavior with non-local dissipation is obtained. By Eq. (33) $\underline{t}=\underline{0}$, $\underline{\underline{\tau}}=\underline{\underline{0}}$ but

$$\underline{\underline{\kappa}}=\left(\underline{\underline{\underline{\Sigma}}}\cdot\underline{\nabla}-\frac{\partial\phi}{\partial\underline{\underline{\beta}}_\mathrm{p}}\right)=\Lambda\frac{\partial\mathscr{d}}{\partial\dot{\underline{\underline{\beta}}}_\mathrm{p}}\quad,\quad\underline{\underline{\underline{T}}}=\left(\underline{\underline{\underline{\Sigma}}}+\frac{\partial\phi}{\partial\underline{\underline{\alpha}}}\cdot\underline{\underline{\underline{\epsilon}}}\right)=\Lambda\frac{\partial\mathscr{d}}{\partial\operatorname{grad}\dot{\underline{\underline{\beta}}}_\mathrm{p}}. \tag{46}$$

Inserting Relation $(43)_2$ into $(43)_1$ yields a partial differential equation for the primary variable $\underline{\underline{\beta}}_\mathrm{p}$:

$$\left(\Lambda\frac{\partial\mathscr{d}}{\partial\operatorname{grad}\dot{\underline{\underline{\beta}}}_\mathrm{p}}-\frac{\partial\phi}{\partial\underline{\underline{\alpha}}}\cdot\underline{\underline{\underline{\epsilon}}}\right)\cdot\underline{\nabla}-\frac{\partial\phi}{\partial\underline{\underline{\beta}}_\mathrm{p}}=\Lambda\frac{\partial\mathscr{d}}{\partial\dot{\underline{\underline{\beta}}}_\mathrm{p}}. \tag{47}$$

Re-arranging the terms and using the fact that the multiplier Λ is constant, we obtain a partial differential equation for the primary variable $\underline{\underline{\beta}}_\mathrm{p}$:

$$-\left(\frac{\partial\phi}{\partial\underline{\underline{\beta}}_\mathrm{p}}+\operatorname{curl}\left(\frac{\partial\phi}{\partial\operatorname{curl}\underline{\underline{\beta}}_\mathrm{p}}\right)\right)=\Lambda\left(\frac{\partial\mathscr{d}}{\partial\dot{\underline{\underline{\beta}}}_\mathrm{p}}-\operatorname{div}\left(\frac{\partial\mathscr{d}}{\partial\operatorname{grad}\dot{\underline{\underline{\beta}}}_\mathrm{p}}\right)\right). \tag{48}$$

Identifying the terms on both sides as the (negative) variational derivatives of ϕ and $\mathscr{d}$, respectively (cf. Sect. 3.2), we find a new Biot-type differential equation [7]:

$$-\frac{\delta\phi}{\delta\underline{\underline{\beta}}_\mathrm{p}}=\Lambda\frac{\delta\mathscr{d}}{\delta\dot{\underline{\underline{\beta}}}_\mathrm{p}}. \tag{49}$$

As this sort of non-local dissipation is not investigated in this study, it shall not be further discussed at this point.

5 Field equations of a continuously dislocated single crystal under single slip

This section aims to derive the governing field equations under single plastic slip conditions, i.e., there is only one active slip system such that the plastic distortion tensor is described by

$$\underline{\underline{\beta}}_\mathrm{p}=\beta_\mathrm{p}(\underline{r})\,\underline{s}\otimes\underline{m}\quad\text{with}\quad\underline{s}\perp\underline{m}, \tag{50}$$

where the slip direction $\underline{s}$ and slip plane normal $\underline{m}$ are constant unit vectors. They depend on the crystallographic directions which are considered as being constant during the deformation.[15] From Eq. (50) the dislocation tensor and the scalar dislocation density follow straightforwardly:

$$\underline{\underline{\alpha}} = \operatorname{curl}(\underline{\underline{\beta}}_{\mathrm{p}}) = \left(\underline{\nabla} \times \underline{\underline{\beta}}_{\mathrm{p}}^{\mathrm{T}}\right)^{\mathrm{T}} = -\underline{\underline{\beta}}_{\mathrm{p}} \times \underline{\nabla} = \underline{s} \otimes \underline{\nabla}\beta_{\mathrm{p}} \times \underline{m}, \tag{51}$$

$$\rho_{\mathrm{d}} = \tfrac{1}{b}\|\underline{\underline{\alpha}}\| = \tfrac{1}{b}|\underline{\nabla}\beta_{\mathrm{p}} \times \underline{m}| = \tfrac{1}{b}|\underline{\nabla}\beta_{\mathrm{p}} \cdot \underline{s}|. \tag{52}$$

The theory is further restricted by only considering the dissipative mechanisms discussed in Sects. 4.4.2 and 4.4.4. Then, the displacement field is ruled by Eq. (37). Due to Constraint (50), the tensor field equation for the plastic distortion reduces to one single scalar field equation which simplifies the theory enormously: Multiplying Eq. (44) or (45) then from the left with $\underline{s}$ and from the right with $\underline{m}$ results in a double contraction into the scalar equation:

$$-\underline{s} \cdot \frac{\delta\phi}{\delta\underline{\underline{\beta}}_{\mathrm{p}}} \cdot \underline{m} = \underline{s} \cdot \Lambda \frac{\partial \mathscr{d}}{\partial \dot{\underline{\underline{\beta}}}_{\mathrm{p}}} \cdot \underline{m} \quad \rightarrow \quad -\frac{\partial\phi}{\partial\beta_{\mathrm{p}}} + \operatorname{div}\left(\frac{\partial\phi}{\partial\underline{\nabla}\beta_{\mathrm{p}}}\right) = \Lambda \frac{\partial \mathscr{d}}{\partial\dot{\beta}_{\mathrm{p}}}. \tag{53}$$

In preparation for the next subsections, let us also calculate the required partial derivatives of the free-energy density. Recall Eqs. (3), (9) and (10), then:

$$\frac{\partial\phi}{\partial\underline{\underline{\beta}}} \overset{(10)}{=} \frac{\partial\phi}{\partial\underline{\underline{\beta}}_{\mathrm{e}}} = \frac{\partial\phi_{\mathrm{e}}(\underline{\underline{\varepsilon}}_{\mathrm{e}})}{\partial\underline{\underline{\varepsilon}}_{\mathrm{e}}} = 2\mu\underline{\underline{\varepsilon}}_{\mathrm{e}} + \lambda(\underline{\underline{\varepsilon}}_{\mathrm{e}} \cdot\cdot\, \underline{\underline{I}})\,\underline{\underline{I}}, \tag{54}$$

$$\frac{\partial\phi}{\partial\underline{\underline{\beta}}_{\mathrm{p}}} \overset{(9)}{=} -\frac{\partial\phi}{\partial\underline{\underline{\beta}}_{\mathrm{e}}} = -\frac{\partial\phi}{\partial\underline{\underline{\beta}}} \quad \Rightarrow -\frac{\partial\phi}{\partial\beta_{\mathrm{p}}} = \underline{s} \cdot \frac{\partial\phi}{\partial\underline{\underline{\beta}}} \cdot \underline{m}. \tag{55}$$

From Definition (50) follows that the plastic distortion is isochoric, i.e., for small deformations $\underline{\underline{\beta}}_p$ is traceless. Hence, Relationship (54) can be further simplified to

$$\frac{\partial\phi}{\partial\underline{\underline{\beta}}} = 2\mu\,\operatorname{sym}(\operatorname{grad}(\underline{u}) - \underline{\underline{\beta}}_{\mathrm{p}}) + \lambda(\operatorname{grad}(\underline{u}) \cdot\cdot\, \underline{\underline{I}})\,\underline{\underline{I}} \tag{56}$$

$$= 2\mu\,\operatorname{sym}\{(\underline{\nabla} \otimes \underline{u})^{\mathrm{T}} - \underline{\underline{\beta}}_{\mathrm{p}}\} + \lambda(\underline{\nabla} \cdot \underline{u})\,\underline{\underline{I}}. \tag{57}$$

Finally, the partial derivative of the free energy with respect to the gradient of the plastic slip is calculated. Introducing the dimensionless dislocation density $v := \rho_{\mathrm{d}}/\rho_{\mathrm{s}}$ gives

$$\frac{\partial\phi}{\partial\underline{\nabla}\beta_{\mathrm{p}}} = \frac{\partial\phi}{\partial v}\frac{\partial v}{\partial\underline{\nabla}\beta_{\mathrm{p}}} \overset{(11)}{=} \frac{k\mu}{(b\rho_{\mathrm{s}})^2}\left(v - v^2\right)^{-1} \underline{s} \otimes \underline{s} \cdot \underline{\nabla}\beta_{\mathrm{p}}. \tag{58}$$

5.1 Simple quadratic dissipation potential and stability analysis

Consider the dissipative mechanisms discussed in Sects. 4.4.2 and 4.4.4 together. To be precise, assume a simple quadratic form of the dissipation potential:

$$\mathscr{d} = \eta_{\mathrm{u}}\dot{\underline{u}} \cdot \dot{\underline{u}} + \eta_{\mathrm{p}}\dot{\beta}_{\mathrm{p}}^2, \quad \Lambda = 1/2. \tag{59}$$

The second term in the potential represents the dissipation due to the viscous interaction of moving dislocations and the atomic lattice. As this microstructural process depends on the velocity of the dislocations, the continuum theory dealing with the collective motion of dislocations becomes *dependent* on the plastic deformation rate. Evaluating Eqs. (39) and (44) under Assumptions (53) and (54) and with Dissipation (59) yields

$$-\frac{\delta\phi}{\delta\underline{u}} \equiv \operatorname{div}(\underline{\underline{\sigma}}) \equiv \operatorname{div}\left(\frac{\partial\phi}{\partial\underline{\underline{\beta}}}\right) = \Lambda\frac{\partial \mathscr{d}}{\partial\dot{\underline{u}}} \equiv \eta_{\mathrm{u}}\dot{\underline{u}}, \tag{60a}$$

$$-\frac{\delta\phi}{\delta\beta_{\mathrm{p}}} \equiv \underline{s} \cdot \underline{\underline{\sigma}} \cdot \underline{m} + \operatorname{div}\left(\frac{\partial\phi}{\partial\underline{\nabla}\beta_{\mathrm{p}}}\right) = \Lambda\frac{\partial \mathscr{d}}{\partial\dot{\beta}_{\mathrm{p}}} \equiv \eta_{\mathrm{p}}\dot{\beta}_{\mathrm{p}}, \tag{60b}$$

[15] This is only valid for small elastic deformations and rigid body rotations. Otherwise, $\underline{s}$ and $\underline{m}$ change during the deformation process.

where the similar structure of both field equations already becomes visible. Moreover, quadratic dissipation potentials obviously lead to field equations analogous to the phase field approach (cf. Sect. 3.3). Consequently, both fields, the displacement and the plastic distortion, evolve in such a way that the free energy is minimized. Inserting the stress field in Form (57) and introducing the constant slip system tensor $\underline{\underline{G}} := \underline{s} \otimes \underline{m}$ finally yields the desired partial differential equations (PDEs) for the multi-field problem:

$$(\lambda + \mu)\underline{\nabla}\otimes\underline{\nabla} \cdot \underline{u} + \mu\underline{\nabla}\cdot\underline{\nabla} \otimes \underline{u} - 2\mu\, \mathrm{sym}(\underline{\underline{G}}) \cdot \underline{\nabla}\beta_\mathrm{p} = \eta_\mathrm{u}\dot{\underline{u}}, \tag{61a}$$

$$2\mu\, \mathrm{sym}(\underline{\underline{G}}) \cdot\cdot\, \underline{\nabla}\otimes\underline{u} - \mu\beta_\mathrm{p} + \frac{k\mu}{(b\rho_\mathrm{s})^2}\left(1 - \frac{|\underline{\nabla}\beta_\mathrm{p}\cdot\underline{s}|}{b\rho_\mathrm{s}}\right)^{-2} \underline{s}\cdot\underline{\nabla}\otimes\underline{\nabla}\beta_\mathrm{p}\cdot\underline{s} = \eta_\mathrm{p}\dot{\beta}_\mathrm{p}. \tag{61b}$$

More details concerning the derivation of Eq. (61b) are given in "Appendix B."

Introducing the directional derivative operator $\underline{D}$, the Laplace operators Δ, $\overset{s}{\Delta}$ and the constant C are defined as follows:

$$\underline{D} := 2\,\mathrm{sym}(\underline{\underline{G}}) \cdot \underline{\nabla}\,, \quad \Delta := \underline{\nabla}\cdot\underline{\nabla}\,, \quad \overset{s}{\Delta} := \underline{s}\cdot\underline{\nabla}\otimes\underline{\nabla}\cdot\underline{s}\,, \quad C = \frac{k\mu}{(b\rho_\mathrm{s})^2}, \tag{62}$$

System (61) can be rewritten in a very compact form which reveals the interesting structure of the PDEs:

$$(\lambda + \mu)\underline{\nabla}\otimes\underline{\nabla} \cdot \underline{u} + \mu\Delta\underline{u} - \mu\underline{D}\beta_\mathrm{p} = \eta_\mathrm{u}\dot{\underline{u}}, \tag{63a}$$

$$-\mu\beta_\mathrm{p} + C\left(1 - \frac{|\underline{\nabla}\beta_\mathrm{p}\cdot\underline{s}|}{b\rho_\mathrm{s}}\right)^{-2} \overset{s}{\Delta}\beta_\mathrm{p} + \mu\underline{D}\cdot\underline{u} = \eta_\mathrm{p}\dot{\beta}_\mathrm{p}. \tag{63b}$$

Equation (63a) is parabolic and linear, whereas Eq. (63b) is nonlinear due to the term in round brackets. Furthermore, the operator $\underline{D}$ imparts the interaction between the two primary fields. Setting the corresponding interaction terms off, the uncoupled equations are a starting point for a simplified stability analysis with the perturbation method. Therefore, a solution of the following form is inserted:

$$\underline{u} = \underline{u}_0 + \hat{\underline{u}}\ \exp(i\,\underline{w}\cdot\underline{r} - \omega_\mathrm{u}t), \tag{64a}$$

$$\beta_\mathrm{p} = \beta_0 + \hat{\beta}_\mathrm{p}\exp(i\,\underline{w}\cdot\underline{r} - \omega_\mathrm{p}t), \tag{64b}$$

with the imaginary unit $i = \sqrt{-1}$, the wave vector $\underline{w} = 2\pi\,\underline{n}/L$ containing the wave length L and propagation direction $\underline{n}$ as well as some unknown angular frequencies ω_u, ω_p. The perturbation is then performed around the local stationary point characterized by $\underline{u}_0 = \text{const.}$ and $\beta_0 = 0$. Considering that the perturbations are small, i.e., $\hat{\underline{u}} \to \underline{0}$ and $\hat{\beta}_\mathrm{p} \to 0$, System (63) can be linearized and the exponential function can be factored out. In case of the displacement field, this procedure leads to an eigenvalue problem with ω_u being the eigenvalues to be determined. The standard procedure then yields:

$$\omega_{\mathrm{u}1} = \left(\frac{2\pi}{L}\right)^2 \frac{(\lambda + 2\mu)}{\eta_\mathrm{u}}, \quad \omega_{\mathrm{u}2,3} = \left(\frac{2\pi}{L}\right)^2 \frac{\mu}{\eta_\mathrm{u}}. \tag{65}$$

For the plastic distortion, the eigenvalue problem reduces to a linear equation from which ω_p is determined as

$$\omega_\mathrm{p} = \frac{\mu}{\eta_\mathrm{p}}\left[1 + k\left(\frac{2\pi}{L}\frac{\underline{n}\cdot\underline{s}}{b\rho_\mathrm{s}}\right)^2\right] = \frac{\mu}{\eta_\mathrm{p}}\left[1 + k\left(2\pi\frac{L_\mathrm{in}}{L}\underline{n}\cdot\underline{s}\right)^2\right]. \tag{66}$$

As all frequencies are real and greater than zero, the temporal behavior for $\underline{D} = \underline{0}$ is simply an exponential decay of the Perturbation (64). Hence, ω_u, ω_p have the physical significance of decay rates. In other words, the local fixed point solution $\underline{u}_0 = \text{const.}$, $\beta_0 = 0$ is *stable*. However, the rate of decay depends on the wave length L: Short waves decay faster than long waves (a.k.a dispersion). Interestingly, the angular frequency ω_p of the plastic distortion field depends on the angle between plastic slip direction $\underline{s}$ and wave propagation direction $\underline{n}$. In addition, ω_p also depends on some length scale $L_\mathrm{in} = 1/(b\rho_\mathrm{s})$. This effect results from the dislocation energy (11), where the internal length was implicitly introduced in the theory. For further discussion, see Sect. 6.4.4.

5.2 Extended dissipation potential and relations to phenomenological viscoplasticity

It is well known that dislocations only move within some slip plane if a critical resolved shear stress τ_{cr} (the so-called Peierls barrier) is exceeded. To consider this effect as well, Dissipation Potential (59) is extended:[16]

$$\mathscr{d} = \eta_{\mathrm{u}} \dot{\underline{u}} \cdot \dot{\underline{u}} + 2\tau_{\mathrm{cr}} |\dot{\beta}_{\mathrm{p}}| + \eta_{\mathrm{p}} \dot{\beta}_{\mathrm{p}}^2, \quad \Lambda = 1/2. \tag{67}$$

At this point, the advantages of the dissipation potential become obvious: Very different dissipative microstructural mechanisms can be captured and the introduced material constants have a clear physical interpretation: the critical resolved shear stress τ_{cr} and the viscosity η_{p} of the collective dislocation motion. Evaluating Field Equation (53) now yields a slightly more complicated form than in Sect. 5.1:

$$\tau_{\mathrm{cr}} \frac{\dot{\beta}_{\mathrm{p}}}{|\dot{\beta}_{\mathrm{p}}|} + \eta_{\mathrm{p}} \dot{\beta}_{\mathrm{p}} = \underline{s} \cdot \underline{\underline{\sigma}} \cdot \underline{m} + \operatorname{div} \left(\frac{\partial \phi}{\partial \underline{\nabla} \beta_{\mathrm{p}}} \right). \tag{68}$$

The plastic slip still evolves in such a way that the free energy is reduced. However, the solution for static equilibrium does not necessarily correspond to an energetic *minimum* anymore. This will become clear in the results presented in Sect. 6. The terms on the right-hand side allow a clear physical interpretation as resolved shear stress τ and resolved backstress τ_{b}, i.e.,

$$\tau \coloneqq \underline{s} \cdot \underline{\underline{\sigma}} \cdot \underline{m}, \quad \tau_{\mathrm{b}} \coloneqq - \operatorname{div} \left(\frac{\partial \phi}{\partial \underline{\nabla} \beta_{\mathrm{p}}} \right). \tag{69}$$

The term "backstress" stems from phenomenological viscoplasticity where the backstress tensor is introduced in order to model kinematic hardening [53]. In statistical mechanics of dislocations, backstresses appear naturally, too [18,22]. Moreover, in the CDT τ is the counterpart of the Peach–Köhler force acting on single, discrete dislocations. The collective dislocation motion within some slip plane is driven by the resolved shear stress. Introducing the effective stress $\tau_{\mathrm{ef}} \coloneqq \tau - \tau_{\mathrm{b}}$, a compact form of Eq. (68) can now be given by

$$\tau_{\mathrm{cr}} \operatorname{sign}(\dot{\beta}_{\mathrm{p}}) + \eta_{\mathrm{p}} \dot{\beta}_{\mathrm{p}} = \tau_{\mathrm{ef}}, \tag{70}$$

where $\dot{\beta}_{\mathrm{p}}/|\dot{\beta}_{\mathrm{p}}|$ was identified with the signum function of $\dot{\beta}_{\mathrm{p}}$. Distinguishing the cases (i) $\tau_{\mathrm{ef}} > \tau_{\mathrm{cr}}$, (ii) $\tau_{\mathrm{ef}} < -\tau_{\mathrm{cr}}$ and (iii) $-\tau_{\mathrm{cr}} \leq \tau_{\mathrm{ef}} \leq \tau_{\mathrm{cr}}$ plus considering that $\operatorname{sign}(0) \in (-1, +1)$, Eq. (70) admits only one solution for determining $\dot{\beta}_{\mathrm{p}}$:

$$\dot{\beta}_{\mathrm{p}} = \frac{\operatorname{sign}(\tau_{\mathrm{ef}})}{\eta_{\mathrm{p}}} \left\langle |\tau_{\mathrm{ef}}| - \tau_{\mathrm{cr}} \right\rangle \tag{71}$$

with the Macauley brackets (a.k.a. Föppl symbol): $\langle x \rangle = x$ for $x > 0$ and otherwise zero. The numerical solution algorithm is as follows:

First assume $\dot{\beta}_{\mathrm{p}} = 0$ (elastic predictor step). Then, two cases are possible:

(1) $|\tau_{\mathrm{ef}}| \leq \tau_{\mathrm{cr}}$: assumption true and $\dot{\beta}_{\mathrm{p}} = 0$
(2) $|\tau_{\mathrm{ef}}| > \tau_{\mathrm{cr}}$: assumption false and $\dot{\beta}_{\mathrm{p}} = \frac{1}{\eta_{\mathrm{p}}} (\tau_{\mathrm{ef}} - \tau_{\mathrm{cr}} \operatorname{sign}(\tau_{\mathrm{ef}}))$
(plastic corrector step)

Field Equation (71) is in fact a flow rule. In pure phenomenological viscoplasticity, a very similar relation called Perzyna's rule is used [49,50,53]. Consequently, the derivation above can be considered as a micromechanical motivation for Perzyna's rule (under the assumption of single slip).[17]

[16] Albeit $\mathscr{d}$ is then not a homogeneous function anymore, the second law in Form (31) is fulfilled since $\mathscr{d}$ is still a positive and convex function.

[17] In contrast to Perzyna's rule, Eq. (71) is a PDE and hence a *non-local* flow rule.

5.3 Boundary conditions

In the present study, first and second kind as well as periodic boundary conditions (BCs) are used.
First kind BCs (a.k.a. Dirichlet BCs) mean that primary variables are prescribed at some boundary $\mathcal{B}$, i.e.,

$$\underline{u}\big|_{\mathcal{B}} = \underline{u}^{\mathcal{B}}, \tag{72a}$$

$$\underline{\underline{\beta}}_{\mathrm{p}}\big|_{\mathcal{B}} = \underline{\underline{\beta}}_{\mathrm{p}}^{\mathcal{B}} \overset{(50)}{\rightarrow} \beta_{\mathrm{p}}\big|_{\mathcal{B}} = \beta_{\mathrm{p}}^{\mathcal{B}}. \tag{72b}$$

Second kind BCs (a.k.a. Neumann BCs) mean that partial derivatives of the primary variables are prescribed at some boundary $\mathcal{B}$. If they are zero, this special sort of boundary condition is called *free* BC:

$$\frac{\partial \phi}{\partial \underline{\underline{\beta}}} \cdot \underline{n}\bigg|_{\mathcal{B}} = \underline{0} \quad \rightarrow \quad \underline{\underline{\sigma}} \cdot \underline{n}\big|_{\mathcal{B}} = \underline{0}, \tag{73a}$$

$$\frac{\partial \phi}{\partial \underline{\underline{\alpha}}} \times \underline{n}\bigg|_{\mathcal{B}} = \underline{\underline{0}} \quad \rightarrow \quad \underline{\underline{\underline{\Sigma}}} \cdot \underline{n}\big|_{\mathcal{B}} = \underline{\underline{0}}. \tag{73b}$$

This BC type was already derived in Sect. 3.2 using the calculus of variation. For the special case of one active slip system, BCs (73) simplify to

$$\underline{\underline{\sigma}} \cdot \underline{n}\big|_{\mathcal{B}} = \mathrm{sym}(\underline{\nabla} \otimes \underline{u} + \beta_{\mathrm{p}}\, \underline{s} \otimes \underline{m}) \cdot \underline{n} + \tfrac{\lambda}{\mu}(\underline{\nabla} \cdot \underline{u})\underline{n}\big|_{\mathcal{B}} = \underline{0}, \tag{74a}$$

$$\underline{\underline{\underline{\Sigma}}} \cdot \underline{n}\big|_{\mathcal{B}} = (\underline{s} \otimes \underline{m})\, \underline{\nabla}\beta_{\mathrm{p}} \cdot (\underline{s} \otimes \underline{s}) \cdot \underline{n}\big|_{\mathcal{B}} = \underline{\underline{0}}. \tag{74b}$$

These free BCs can be interpreted in the following way: BC (73a) means the stress vector $\underline{s} = \underline{0}$ at the boundary (zero traction) and BC (73b) means $\underline{\underline{S}} = \underline{\underline{0}}$ at the boundary (cf. Eq. (24)). The latter condition implies that dislocations can pass the boundary of the domain. This seems to be reasonable whenever there is a free surface of the crystal. The situation is completely different for (high angle) grain boundaries, which are in general non-permeable for dislocations. Then, dislocations cannot pass this boundary and hence the plastic distortion is zero at the boundary. Consequently, BC (72b) should be used with $\beta_{\mathrm{p}}^{\mathcal{B}} = 0$.[18] Consider another case when a (single) crystal is clamped by a "hard device." Such a fixed bearing is used to prescribe the displacement on the boundary. Consequently, the first kind BC (72a) must be applied for the displacement. However, demanding the same BC (72b) for the plastic distortion seems too strict. From the microstructural point of view it cannot be expected that no dislocations leave the crystal anymore. Therefore, the following mixed BCs are applied in the case of a "hard device":

$$\underline{u}\big|_{\mathcal{B}} = \underline{u}^{\mathcal{B}}(t), \tag{75a}$$

$$(\underline{\nabla}\beta_{\mathrm{p}} \cdot \underline{s})(\underline{s} \cdot \underline{n})\big|_{\mathcal{B}} = 0. \tag{75b}$$

Periodic BCs are useful when surface effects are not desired. The body is considered to be composed of repetitive parts, and hence, all primary field variables have periodical properties. The boundary in some negative coordinate direction is denoted by $\mathcal{B}^-$, and the boundary with opposing normal after some space interval $\Delta\underline{r}$ of periodicity is denoted by $\mathcal{B}^+$. Periodic BCs then read

$$\underline{u}\big|_{\mathcal{B}^+} = \underline{u}\big|_{\mathcal{B}^-} + \underline{\underline{H}} \cdot \Delta\underline{r}, \tag{76a}$$

$$\underline{\underline{\beta}}_{\mathrm{p}}\big|_{\mathcal{B}^+} = \underline{\underline{\beta}}_{\mathrm{p}}\big|_{\mathcal{B}^-} \overset{(50)}{\rightarrow} \beta_{\mathrm{p}}\big|_{\mathcal{B}^+} = \beta_{\mathrm{p}}\big|_{\mathcal{B}^-}, \tag{76b}$$

where $\underline{\underline{H}}$ has the meaning of some constant displacement gradient controlling the average affine deformation.

[18] This provokes high dislocation densities near grain boundaries and also high stresses since the total deformation can be only elastic there.

6 Numerical simulations for plane strain state and single slip

6.1 Initial boundary value problem for plane strain and edge dislocations

The initial boundary value problem consists of the partial differential equations from Sect. 5.2 (including Sect. 5.1 as special case), the boundary conditions from Sect. 5.3 and some initial conditions (ICs) for the two primary fields:

$$\underline{u}(t=0,\underline{r}) = \underline{u}^0, \quad \beta_\mathrm{p}(t=0,\underline{r}) = \beta_\mathrm{p}^0. \tag{77}$$

The third displacement component is set to zero which leads to the special case of a plane displacement field (cf. also [20]):

$$\underline{u}(t,\underline{r}) = u_x(t,x,y)\,\underline{e}_x + u_y(t,x,y)\,\underline{e}_y, \quad \beta_\mathrm{p}(t,\underline{r}) = \beta_\mathrm{p}(t,x,y). \tag{78}$$

In addition, direction $\underline{s}$ and normal $\underline{m}$ of plastic slip are assumed to lie within this deformation plane, oriented at some angle φ (cf. Fig. 6 in Sect. 6.4):

$$\underline{s} = \cos\varphi\,\underline{e}_x + \sin\varphi\,\underline{e}_y, \quad \underline{m} = -\sin\varphi\,\underline{e}_x + \cos\varphi\,\underline{e}_y. \tag{79}$$

Remark 4 Implicitly, Assumptions $(78)_2$ and (79) implicate the character of dislocations involved. As recapitulated in Sect. 2.1, the dislocation tensor is composed of dyadic products of Burgers vectors and tangent vectors of line segments. Comparing Eqs. (1) and (51), it is obvious that the resultant Burgers vector is proportional to the slip direction $\underline{s}$. Furthermore, the cross product $\underline{\nabla}\beta_\mathrm{p} \times \underline{m}$ defines the (mean) tangent direction $\underline{t}_\mathrm{r}$ of the continuously distributed dislocations. In the special case considered here, $\underline{t}_\mathrm{r} \sim \underline{\nabla}\beta_\mathrm{p} \times \underline{m} \sim \underline{e}_z$. Consequently, $\underline{b}_\mathrm{r} \perp \underline{t}_\mathrm{r}$ and the dislocation lines are of *straight edge* type.[19]

System (63) (and also the more general Eq. (70)) and ICs plus constraints given in this subsection and BCs given in Sect. 5.3 represent the strong formulation of the two-dimensional problem. It was solved numerically using the finite difference method with explicit time stepping.

6.2 Explicit finite difference implementation

The finite difference method (FDM) approximates partial derivatives (with respect to time and space coordinates) as difference quotients. In the present study, central difference quotients were used for partial derivatives with respect to space coordinates. In order to obtain explicit update formulas, forward difference quotients were used for partial derivatives with respect to time. Furthermore, the space time continuum was discretized by introducing a number of $N_x \cdot N_y$ space intervals of equal size Δx, Δy and N_t time intervals of equal size Δt with t_n denoting the nth time step and $\underline{u}(t_n,\underline{r}) = \underline{u}^n$. The time-discretized version of the partial differential equations is given for the model from Sect. 5.2 (including 5.1 as special case for $\tau_\mathrm{cr} = 0$):

$$\underline{u}^n = \underline{u}^{n-1} + \frac{\Delta t}{\eta_\mathrm{u}}\Big[(\lambda+\mu)\underline{\nabla}\otimes\underline{\nabla}\cdot\underline{u}^{n-1} + \mu\Delta\underline{u}^{n-1} - \mu\underline{D}\beta_\mathrm{p}^{n-1}\Big], \tag{80a}$$

$$\beta_\mathrm{p}^n = \beta_\mathrm{p}^{n-1} + \mathrm{sign}\left(\tau_\mathrm{ef}^{n-1}\right)\frac{\Delta t}{\eta_\mathrm{p}}\left\langle|\tau_\mathrm{ef}^{n-1}| - \tau_\mathrm{cr}\right\rangle \tag{80b}$$

$$\text{with } \tau_\mathrm{ef}^{n-1} = \tau^{n-1} - \tau_\mathrm{b}^{n-1} = \mu(\underline{D}\cdot\underline{u}^{n-1} - \beta_\mathrm{p}^{n-1}) + C\left(1 - \frac{|\underline{\nabla}\beta_\mathrm{p}^{n-1}\cdot\underline{s}|}{b\rho_\mathrm{s}}\right)^{-2}\overset{s}{\Delta}\beta_\mathrm{p}^{n-1}.$$

The numerical solution algorithm for System (80) now distinguishes different cases with respect to the rate dependence controlled by η_u and η_p.

Rate dependence of plastic slip and displacement Having defined ICs and BCs, System (80) can be solved on a grid using the FDM. In this case, the temporal evolution of the primary fields toward the equilibrium state ($\dot{\underline{u}} = \underline{0}, \dot{\beta}_p = 0$) may be followed. The kinetics are equal to a simple phase field approach where the system evolves "down the energy gradient," as given in Sect. 3.3. As the damping constant η_u lacks a physical

[19] Straight *screw* dislocations are possible as well within this framework. However, then the problem becomes "anti-plane" and there is no plane strain state anymore [6].

meaning, the evolution toward equilibrium should not be over-interpreted. Nevertheless, it is interesting to have a look at this relaxation as will be done in Sect. 6.4.4.

Rate independence Theoretically, the right side of, e.g., System (63) is zero now, and thus, a static equilibrium solution is sought-after. However, the discretized Form (80) can still be used: The loading of the system is subdivided into small load steps prescribed by time-dependent BCs. Within each load step, a relaxation toward the temporal equilibrium is performed. The parameters η_u, η_p have no physical meaning and are estimated in such a way that the largest increments can be achieved: The time and space periods (T, L) appearing in Formulas (65) and (66) need to be resolved with a sufficient number of points in time (M_t) and space (M), i.e., $T_u \equiv 2\pi/\omega_{\mathrm{u}1} = M_t \Delta t$, $T_\mathrm{p} \equiv 2\pi/\omega_\mathrm{p} = M_t \Delta t$ and $L^2 = M^2 \Delta x \Delta y$. This poses constraints on the viscosities as:

$$\eta_\mathrm{u} = 2\pi \frac{(\lambda + 2\mu) M_t \Delta t}{M^2 \Delta x \Delta y}, \quad \eta_\mathrm{p} = \frac{\mu M_t \Delta t}{2\pi} \left[1 + k \left(\frac{2\pi}{M} \right)^2 \frac{L_\mathrm{in}^2}{\Delta x \Delta y} \right], \tag{81}$$

where $\underline{n}$ was assumed parallel to $\underline{s}$. It was found numerically that $M \geq 2\pi$ and $M_t \geq 5M$ leads to a stable integration and accurate numerical results. Thus, a lower bound for the viscosities is obtained:

$$\eta_\mathrm{u} = 5 \frac{(\lambda + 2\mu) \Delta t}{\Delta x \Delta y}, \quad \eta_\mathrm{p} = 5 \frac{\mu \Delta t}{2\pi} \left[1 + k \frac{L_\mathrm{in}^2}{\Delta x \Delta y} \right]. \tag{82}$$

Using the lower bounds of the viscosities, which corresponds to the choice $M = 2\pi$, $M_t = 10\pi$, results in the fastest possible relaxation toward the static equilibrium. Mathematically speaking, this algorithm emulates the solution of the system of equations obtained applying *implicit* time integration but avoids assembling system matrices. Most importantly, the code is very flexible and facilitates testing different models derived from the presented CDT, as given in Sect. 5.

Rate dependence of plastic slip As discussed in Sect. 5.1, η_p represents the viscous interaction of dislocations and crystal lattice. It may be estimated employing atomistic models such as molecular dynamics. In this case, Eq. (80b) can be solved straightforwardly whereas for the displacement field a relaxation is performed within each time step until $\underline{u}^n$ does not change anymore.

6.3 Verification of the explicit FDM solution algorithm

In order to verify the in-house finite difference code, a benchmark problem with a known analytical solution was considered: A thin strip under plane confined shear [38]. Since the width and length of the strip are much larger than its height h, plane strain conditions can be assumed and the problem reduces to two dimensions (x and y), as shown in Fig. 4.

In order to prescribe the shear, first kind BCs (72) with $\underline{u}^{\mathcal{B}} = \gamma(t) h \underline{e}_x$ and $\beta_\mathrm{p}^{\mathcal{B}} = 0$ were used in y-direction at $y = 0$ and $y = h = 1\mu\mathrm{m}$, as shown in Fig. 4. Since the solution shall only depend on the y-coordinate, periodic BCs (76) were applied in the x-direction. Hence, $N_x = 2$ was sufficient, whereas the number of discretization points in the y-direction was varied between $N_y = 10$ and 200. The total simulation time was $\mathrm{T_{tot}} = 0.4\mathrm{ms}$, with $N_t = 2000$ time steps. The material parameters were taken from [38], and rate independence was assumed (cf. Sect. 6.2). The evolution of the plastic slip is depicted in Fig. 5 and compared to the plateau value in the middle section calculated analytically. It is important to note that the analytical solution was obtained from the *weak* formulation of the problem (cf. Eq. (16)) by variational methods. In contrast to

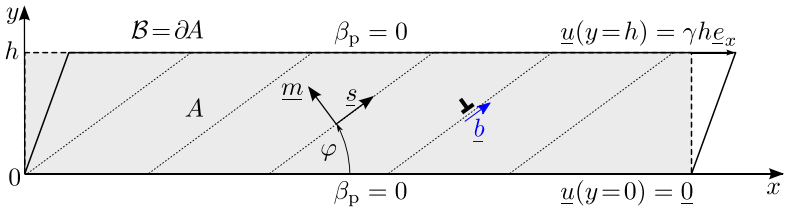

Fig. 4 Plane strain shear of a thin strip [38]: Representatively for the type of continuously distributed dislocations, a straight edge dislocation and some slip planes (dashed) are shown

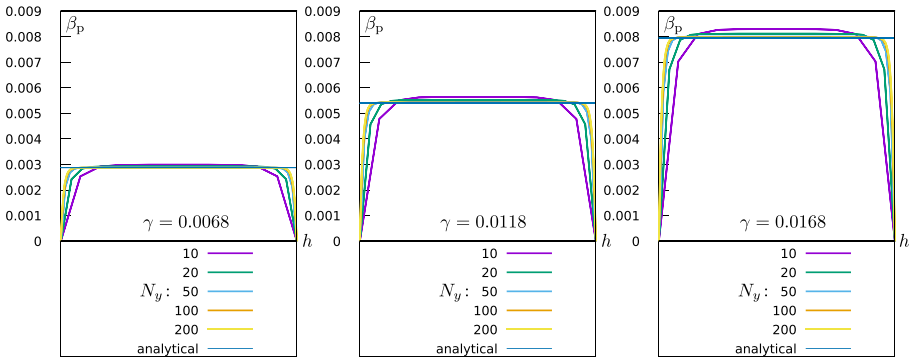

Fig. 5 Different stages of the evolution of the plastic slip β_p over the y-coordinate for the slip system orientation $\varphi = 30°$ and $\tau_{cr} = 13.604$MPa according to [38]

that, the starting point for the numerical scheme (80) was the *strong* formulation. However, both solutions are in accurate agreement. Due to the zero-slip BC a narrow boundary layer involving high gradients is forming analogously to a fluid flow with zero-velocity BC. Numerically, this is a challenging problem. However, the convergence of the (strong) numerical solution to the (weak) analytical solution with increasing N_y can be seen clearly, as shown in Fig. 5. Additionally, the width of the boundary layer converges to a constant value which does *not* depend on the discretization anymore for $N_y > 100$. Beyond serving as a sanity check of the code, this benchmark problem has also been used for a comparison to discrete dislocation dynamics (DDD) simulations. It was shown that the analytical solution (and hence also the present numerical solution) from the CDT is in accurate agreement with DDD simulations [38].

6.4 Monotonic and cyclic tests on Al single crystals

The material to be considered in this subsection is pure single-crystal aluminum. The corresponding material parameters are summarized in Table 1.

Table 1 Material parameters for Al single crystals

μ/MPa	λ/MPa	τ_{cr}/MPa	b/µm	ρ_s/µm^{-2}	k
26315.79	51083.59	13.604	2.86×10^{-4}	4×10^{2}	4×10^{-4}

The material parameters for the dislocation ensemble energy can be estimated roughly by the following considerations: Soft annealed metallic crystals have $\rho_d \approx 10^{-2}$µm^{-2}, whereas severely deformed crystals show 10^{4}µm^{-2} [23]. If no further information is available, the saturated dislocation density ρ_s can be chosen close or equal to this upper bound. Here, in the special case of Al crystals, a value in the range suggested by Berdichevsky is used [5]. Parameter k has the meaning of a weighting factor between strain energy and dislocation energy. The size of k is found subject to the condition that the linearization of Eq. (11) has the well-known linear and quadratic dependence on the dislocation density and Burgers vector magnitude, respectively. This leads to

$$\phi_d \approx k\mu \frac{\rho_d}{\rho_s} \stackrel{!}{=} c\mu b^2 \rho_d \quad \text{with} \quad c \in (0, 1]. \tag{83}$$

Hence, $k = cb^2\rho_s$ can be estimated. With k and ρ_s as given in Table 1, the theory's internal length scale $L_{in} = (b\rho_s)^{-1}$ follows as 8.74 µm. The viscosity parameters were chosen according to Sect. 6.2. The body was assumed to occupy a quadratic domain with dimensions $L_x = L_y = 100$ µm, as shown in Fig. 6. Thus, the body is sufficiently larger than its internal length scale. This is important for the investigation of dislocation structures and possible pattern formation.

6.4.1 Monotonic periodic shear test

As a homogeneous test, the body was sheared monotonically, as shown in Fig. 6. To avoid surface effects, periodic BCs (76) were applied and the average displacement gradient $\underline{\underline{H}} = H_{xy}(t)\, \underline{e}_x \otimes \underline{e}_y$ was increased

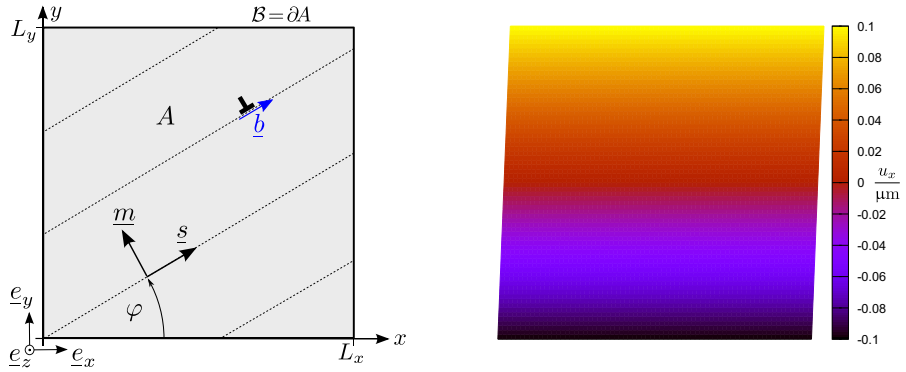

Fig. 6 Quadratic domain left: representatively for the type of the continuously distributed dislocations, a straight edge dislocation with its elementary Burgers vector $\underline{b}$ is shown. Right: displacement field for $\varphi = 0°$, final state plotted on the deformed crystal domain (magnified by a factor of 20): Periodic BCs were applied

linearly up to a magnitude of 2‰. For the discretization, a grid with $N_x \cdot N_y = 70 \cdot 70$ points was used. The total simulation time was $T_{tot} = 1$ ms, with $N_t = 10{,}000$ time steps. Zero initial conditions were used and rate independence was assumed (cf. Sect. 6.2).

The resulting displacement field is perfectly linear with respect to the x-component, as shown in Fig. 6 right, and the y-component is zero. The plastic distortion field $\beta_p(x, y)$ is homogeneous. As there are no gradients in the slip direction, the dislocation density is zero according to Eq. (52). After the critical resolved shear stress (τ_{cr}) is exceeded, the body deforms ideally plastically: There is no resistance to plastic distortion and no hardening (cf. also Fig. 7 for $\varphi = 0°$).

6.4.2 Cyclic periodic shear test

In order to numerically study some dissipation mechanisms from Sect. 4.4, the shear test was used again. The average displacement gradient $\underline{\underline{H}}$ was prescribed as harmonic function with $H_{xy}(t) = 0.003 \sin(\Omega t)$. The angular velocity Ω was chosen such that exactly one hysteresis loop closed within the amount of time. As the primary fields remain linear or constant in these conditions, the domain in Fig. 6 was discretized by a grid of only $N_x \cdot N_y = 12 \cdot 12$ points. The total simulation time was $T_{tot} = 3$ms, with $N_t = 30{,}000$ time steps. Initially, both primary fields were zero. The slip system orientation is $\varphi = 15°$.

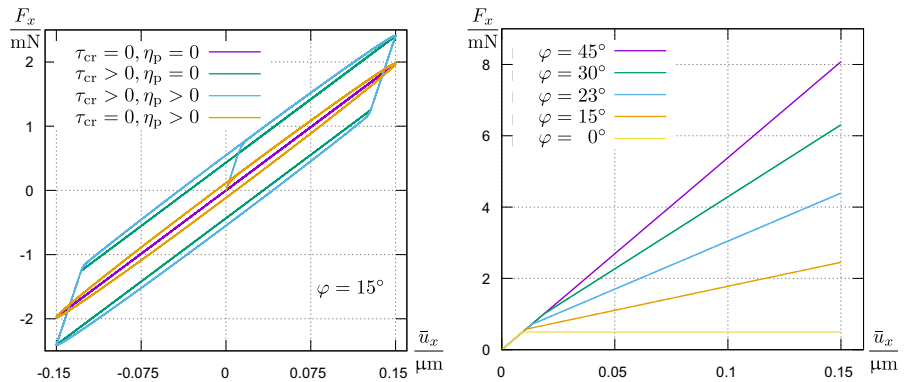

Fig. 7 Force–displacement curves, left: cyclic shear test with different kinds of dissipation. Right: monotonic shear test for different slip system orientations φ

Figure 7 shows the reaction force F_x as a function of the mean displacement $\underline{\bar{u}}$. The force is calculated by integrating the stress vectors on the upper boundary of the quadratic domain:

$$\underline{F} = \int_{x=0}^{L_x} \int_{z=0}^{1\mu m} \underline{\underline{\sigma}}(x, y = L_y) \cdot \underline{e}_y \, dx \, dz \quad \text{and} \quad \underline{\bar{u}} = \frac{1}{L_y} \int_{x=0}^{L_x} \underline{u}(x, L_y) \, dx. \tag{84}$$

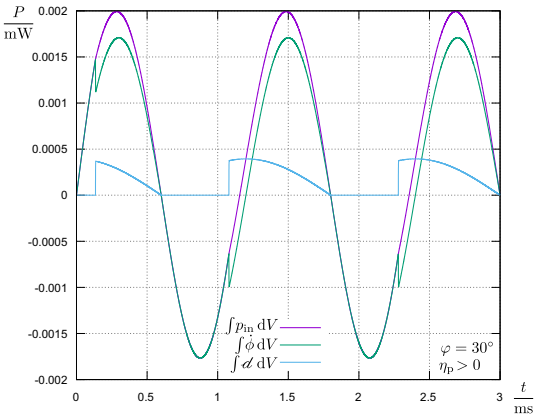

Fig. 8 Total internal power, rate of the free energy and dissipation over the time: There is no dissipation in the elastic stages

In case of zero dissipation ($\eta_\mathrm{p} = \tau_\mathrm{cr} = 0$), the force always follows the same straight line, as shown in Fig. 7 left. Otherwise, hysteresis can be observed. Furthermore, the critical resolved shear stress τ_cr causes a sharp yield limit, as shown in Fig. 7 left. Only in the case $\tau_\mathrm{cr} = 0$ is a smooth transition between elastic and plastic range observed. These results are in perfect agreement with phenomenological viscoplasticity. As the plastic slip is distributed homogeneously, dislocation density and backstress remain zero. Still, a Bauschinger effect similar to kinematic hardening is visible in Fig. 7 left. Looking at the monotonic $F_x(\bar{u}_x)$ curves for different slip system orientations, as shown in Fig. 7 right, it becomes clear that this kind of "hardening" is a pure geometrical effect arising from the anisotropic plastic behavior: In the case of $\varphi = 0$, the total deformation can be realized entirely by plastic slip. For $\varphi > 0$, this is not possible anymore and the crystal (lattice) is strained elastically even in the plastic range. In the "worst case" of $\varphi = 45°$, the slip system is oriented so unfavorably that no plastic deformation is possible, as shown in Fig. 7 right.[20] This is also evident considering the resolved shear stress, which is zero in these slip planes. This behavior is well known as "Schmid's law." Obviously, there is a criterion to distinguish this geometrical effect from work hardening: The observed yield limit is already higher than τ_cr at the beginning of the plastic deformation, as shown in Fig. 7 right, whereas for "real" kinematical hardening the initial yield limit would be exactly the yield stress.

In order to verify the thermodynamical consistency *numerically*, the Clausius–Planck Inequality (27) was evaluated *globally*. Figure 8 shows that the total internal power—which is the external power in the absence of inertia effects—is always greater than or equal to the rate of the free energy. Thus, the amount of energy stored within the material is never greater than the work performed by external forces. The difference is the dissipated energy. During the purely elastic stages of the cyclic deformation, the dissipation is zero. After yielding, the rate of the free energy drops and the dissipation (power) rises abruptly. Physically, the crystal lattice strain is now reduced and the stored energy is released. After the load reversal, the purely elastic regime recurs until τ_cr is exceeded again, yielding sets in and the processes repeat themselves.

6.4.3 Cyclic confined bending tests

In the example from Sect. 6.3, gradients in the field variables resulted merely from the no-slip BC, which produced a boundary layer of finite width. Elsewhere, the plastic slip was homogeneous. As a consequence of the periodic BCs, the shear test in Sect. 6.4.1 was homogeneous as well. Now, a simple example of an inhomogeneous test with *significant inherent* gradients is considered in order to study the evolution of dislocation structures and corresponding hardening effects. Therefore, the displacement $\underline{u}^{\mathcal{B}} = u_x^{\mathcal{B}}(x, y)\sin(\Omega t)\,\underline{e}_x$ is prescribed linearly at the boundary such that the resulting deformation and stress field is similar to bending, as shown in Fig. 9. However, it is neither guaranteed that material cross sections remain plane nor that middle planes are perpendicular to the neutral elastic line. Hence, this case is more general than bending of Timoshenko or Bernoulli type. For $\beta_\mathrm{p}(x, y)$, second kind BCs (74b) are applied.

[20] Within a geometrically *nonlinear* theory, the slip system would be able to rotate such that plastic deformation could take place again.

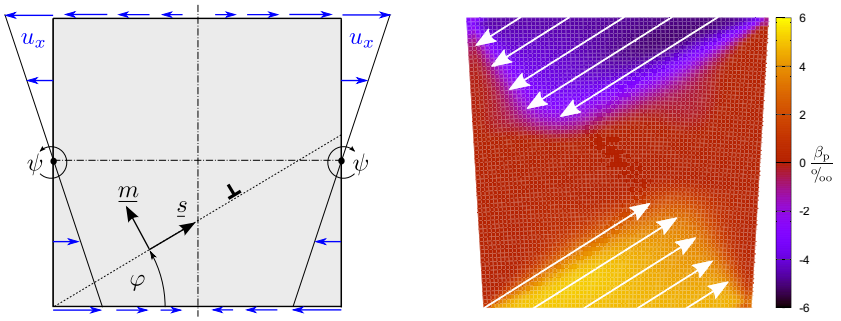

Fig. 9 Cyclic confined bending test setup (left) and plastic slip field (right) for $\varphi = 30°$: The white arrows indicate dislocations that nucleated at the surface and moved to the inside

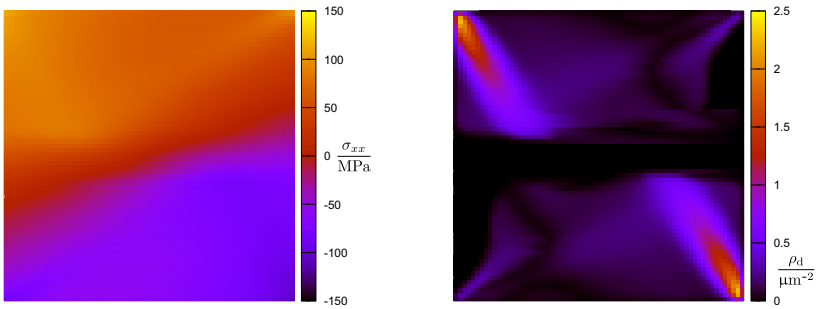

Fig. 10 Bending stress (left) and dislocation density field (right) for $\varphi = 30°$, final state plotted on the *undeformed* crystal domain: σ_{xx} deviates from a linear distribution

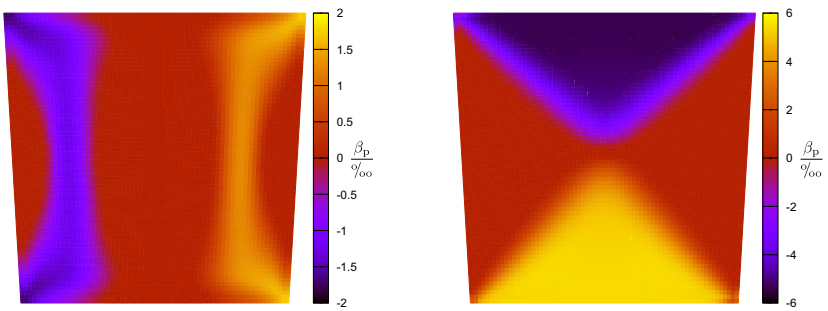

Fig. 11 Plastic slip field $\beta_p/‰$ for $\varphi = 0°$ (left) and $\varphi = 45°$ (right), final state plotted on the *deformed* crystal domain (magnified by a factor of 20): The fields are inhomogeneous

The space discretization was chosen as in Sect. 6.4.1, and the total simulation time was $T_{tot} = 5$ ms with $N_t = 100{,}000$ time steps. Rate independence was assumed (cf. Sect. 6.2). The initial conditions are

$$\underline{u}(t = 0, x, y) = \underline{0}, \quad \beta_p(t = 0, x, y) = \mathrm{rand}(0, 10^{-4}). \tag{85}$$

This means that the single crystal is not displaced initially, but exhibits some very small, random, incompatible plastic deformation. Thus, GNDs already exist in the initial state (cf. also Fig. 14).

The deviation from a linear distribution of the bending stress, as shown in Fig. 10, emerges in the plastic range and is a result of the strongly anisotropic deformation. Furthermore, the plastic slip starts at the upper and lower surface of the body where the resolved shear stress is highest. Physically, dislocations nucleate and start moving until they get stuck at some place inside the crystal where the resolved shear stress is lower than τ_{cr}. This explains the dislocation free zones in Figs. 10 and 12. Moreover, typical dislocation pile-ups can be observed. They are unstable in the sense that after load reversal they break down and eventually emerge again during reloading.

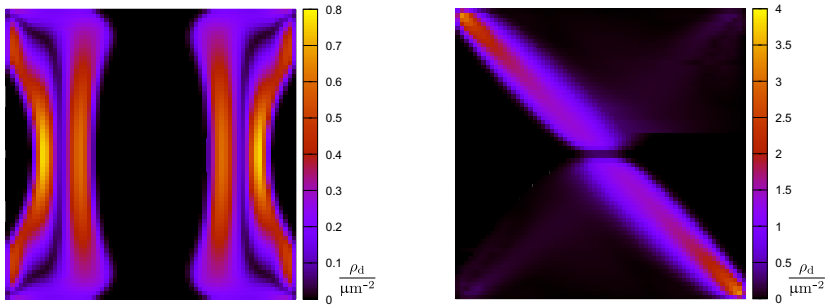

Fig. 12 Dislocation density $\frac{\rho_d}{\mu^{-2}}$ field for $\varphi = 0°$ (left) and $\varphi = 45°$ (right), final state plotted on the *undeformed* crystal domain: Dislocation structures with a high density have emerged

As a consequence of the inhomogeneous solution for the plastic slip, higher-order stresses according to Eq. (58) are present.[21] Thus, the work hardening should be observable. In order to make this effect visible, integral quantities are considered: The reaction moment is calculated by integrating the local moments with respect to some reference point $\underline{r}_0$ over the left boundary of the quadratic domain. The obvious choice for the reference point is the middle of the domain, i.e., $\underline{r}_0 = L_x/2\,\underline{e}_x + L_y/2\,\underline{e}_x$. The reaction moment M_z as a function of the mean bending angle $\bar{\psi}$:

$$\underline{M} = \int_{y=0}^{L_y} \int_{z=0}^{1\mu m} (\underline{r} - \underline{r}_0) \times \underline{\underline{\sigma}}(x{=}0,\, y) \cdot (-\underline{e}_x)\, \mathrm{d}y\, \mathrm{d}z \quad \text{and} \quad \bar{\psi} = \frac{u_x(L_x, L_y, t)}{L_y}, \tag{86}$$

is depicted in Fig. 13. First of all, a smooth elastic–plastic transition is visible. This results from the inhomogeneous onset of yielding. In the case $k = 0$, i.e., the dislocation energy is zero, the backstresses remain zero as well. Still, there is an increase of the moment in the plastic range. This is the geometrical Bauschinger effect explained in the previous subsection. Now using the physically reasonable value $k = 0.0004$ (cf. discussion in Sect. 6.4), the $M_z(\bar{\psi})$ curve is almost indistinguishable from the one for $k = 0$. To see some significant effect under single-slip conditions, unphysically high values of the constant k need to be applied. Hence, this sort of kinematic hardening remains small under normal circumstances and the geometrical Bauschinger effect is much more pronounced. This might change when several slip systems are active and their energetical interaction is taken into account.

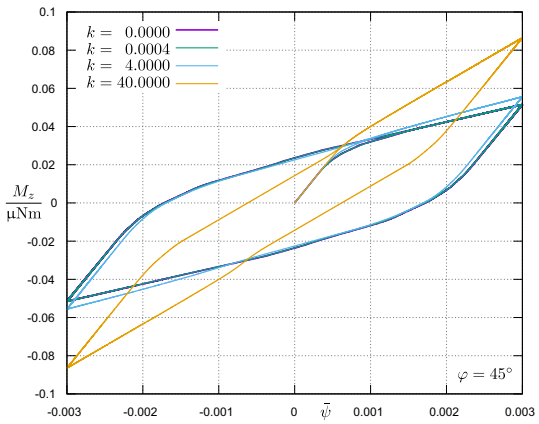

Fig. 13 Bending moment over the mean bending angle for the confined bending test: Hysteresis loops and the effect of constant k are visible

Interestingly, compared to a pure phenomenological anisotropic plasticity model with kinematic hardening, the presented CDT is able to produce two distinct mechanisms that lead to Bauschinger effects.

[21] Flow Rule (71) couples Cauchy stresses and higher-order stresses in the form of τ_{ef}.

6.4.4 Pure relaxation tests with periodic BCs

In order to further investigate the processes during the relaxation phase, a pure relaxation test with periodic BCs was performed for $\tau_{\mathrm{cr}} = 0$. No mechanical loading is prescribed. Both fields, β_{p} and $\underline{u}$, now show rate dependence (cf. Sect. 6.2). The initial conditions are zero displacement and a random distribution of the plastic distortion, as shown in Eq. (85). This perturbed state (cf. Fig. 14, left) is energetically unfavorable, and thus, there is a driving force of the system toward some equilibrium state. Therefore, dislocation patterns emerge, as shown in Figs. 15 and 16.

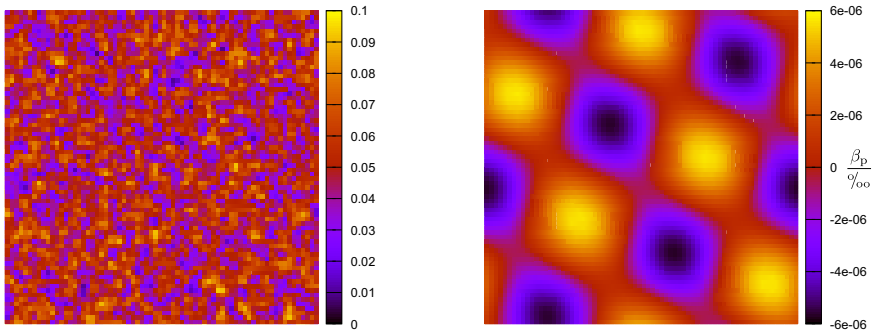

Fig. 14 Initial (left) and final (right) plastic distortion field for $\varphi = 30°$ and periodic BCs

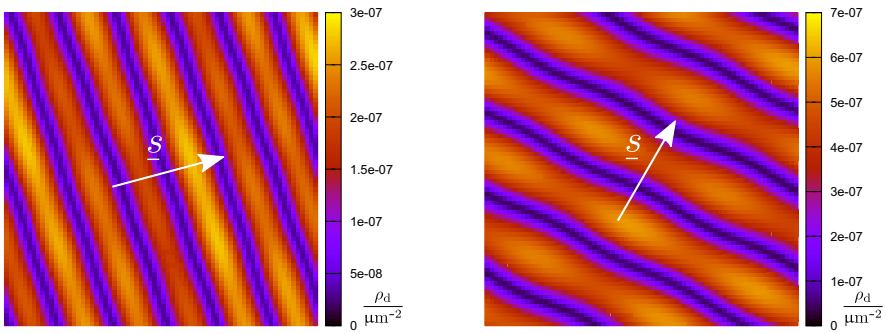

Fig. 15 The dislocation density bands form perpendicular to the slip direction $\underline{s}$

Mathematically speaking, Eq. (63b) [and thus also the more general Eq. (70)] constitutes a strongly anisotropic diffusion problem where the flow is only allowed in one direction—the slip direction $\underline{s}$. In reality, multiple slip systems are active and prevent the crystal from such a strong plastic anisotropy. Nevertheless, the bands shown in Fig. 15 have a physical interpretation: The dislocations are stapled one upon the other perpendicular to $\underline{s}$. This is a consequence of the repelling micro forces (backstresses) acting only in slip direction. From the simplified stability analysis in Sect. 5.1, it can be inferred that perturbations decay exponentially. Indeed, the simulations show that the emerging patterns cannot persist, and they are only transient. Formula (66) gives interesting insights and shows that this extinction is twofold: Firstly, it depends on the scalar product of wave vector and slip direction; secondly, it depends on the quotient of internal length and wavelength. The conclusions are: The mode decays faster the shorter the wave length is. This represents an extinction of modes. Finally, only long waves with a propagation direction perpendicular to the slip direction will be left over, as shown in Fig. 16. Eventually, they fade away too.[22]

If τ_{cr} is taken into account, the extinction of modes will stop when $\tau < \tau_{\mathrm{cr}}$ everywhere. Hence, the pattern, i.e., the dislocation configuration, is frozen.

A desirable comparison with experimental data is difficult since the initial state is somewhat artificial. However, comparable DDD simulations exist, where the relaxation of an initial configuration of edge dislocations was studied [19]: In the relaxed state, the dislocations are stapled one upon the other. This corresponds exactly to the band structure in the presented CDT simulation results. Finally, the dislocation structure shows

[22] The fact that the simulations show exactly this behavior justifies the simplified stability analysis from Sect. 5.1.

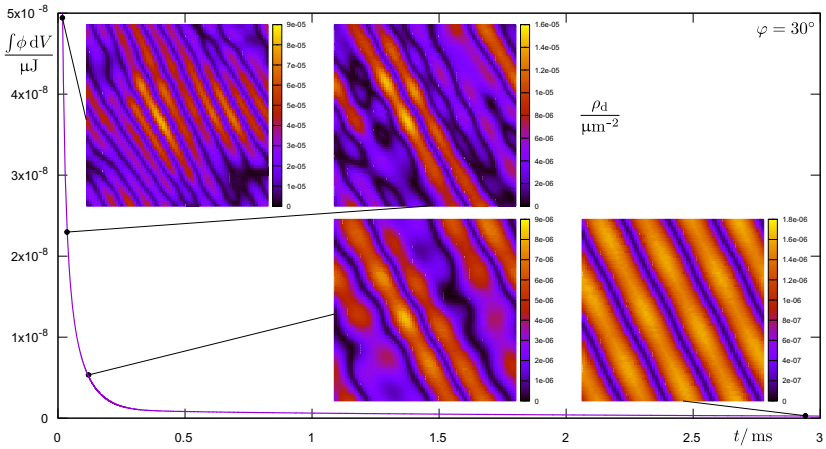

Fig. 16 Evolution of the dislocation density during the relaxation test: As the free energy is reduced steadily, bands with increasing wave length and decreasing amplitude emerge

some similarities with typical dislocation vein structures of single crystals under fatigue loading [55]. There, high dislocation density walls are separated by zones of low dislocation density. The characteristic width of these zones is in the order of μm. This corresponds to the length scale found in the CDT simulations, cf. Figs. 6 and 15. However, persistent slip bands are much more complicated than the presented results. Of course, more effects have to be taken into account in order to realistically simulate the emergence of these structures.

6.5 Monotonic compression tests on Cu single crystals

For the previous test examples, a desirable validation with experimental results was not possible since suitable data could not be found. This is mostly due to the fact that it is very difficult to realize single-slip conditions experimentally. In order to estimate the value of the simulation results, another test is simulated where corresponding experimental data are indeed available: Uniaxial plane strain compression experiments on Cu single crystals were studied thoroughly in a series of papers [13,14,42]. Single-slip conditions were realized insofar as the crystals were oriented to maximize the shear stress in one octahedral slip system. As long as only this primary slip system is active, the experimental results may be compared to simulation results under the single-slip assumption (cf. Eq. (50)).

The crystal dimensions $L_y = 15{,}000\mu m$ and $L_x \approx L_y/3$ (according to [14]) as well as the BCs are depicted in Fig. 17. The boundary of the $u(x, y)$ field has mixed character: On the top and bottom, the displacement is prescribed via first kind BCs (72a), whereas the displacements at the left and right side can adjust freely via second kind BCs (74a). For $\beta_p(x, y)$, only second kind BCs (74b) are applied. The domain in Fig. 17 was discretized by a grid with $N_x \cdot N_y = 36 \cdot 112$ points. The total simulation time was $T_{tot} = 1\,ms$, with $N_t = 10{,}000$ time steps. Initially, both primary fields were zero. The slip system orientation is $\varphi = -45°$. The maximum total compression was set to $-1‰$ and rate-independent behavior of the crystal was assumed. The elastic constants of Cu as well as b and τ_{cr} had to be taken from the literature, as given in Table 2. The remaining constants were estimated in the way explained in Sect. 6.4. For this reason, it can only be expected to *qualitatively* fit the experimental results.

Figure 17 shows the plastic slip field as well as the strain fields for a total compression of $-1‰$. The maximal slip activity is located in the middle of the sample, whereas at the top and bottom the strain remains very small. These simulation results are in perfect agreement with the experimental studies [13,14,42]. The distribution of the compressive strain ε_{yy} accurately fits the experimental results obtained from digital image correlation (cf. Figs. 4, 5 and 6 in [42]).[23]

In order to compare to the experimental displacement field data, the slip direction and normal are used as a natural basis system. Hence, the coefficients of the displacement field read as $u_s = \underline{u} \cdot \underline{s}$ and $u_m = \underline{u} \cdot \underline{m}$.

[23] Unfortunately, the color scale in Fig. 4 [42] is too broad in the small strain regime for a *quantitative* comparison. However, even for moderate strains the experimental results show a very similar distribution compared to the presented numerical results for ε_{xx} and ε_{yy}.

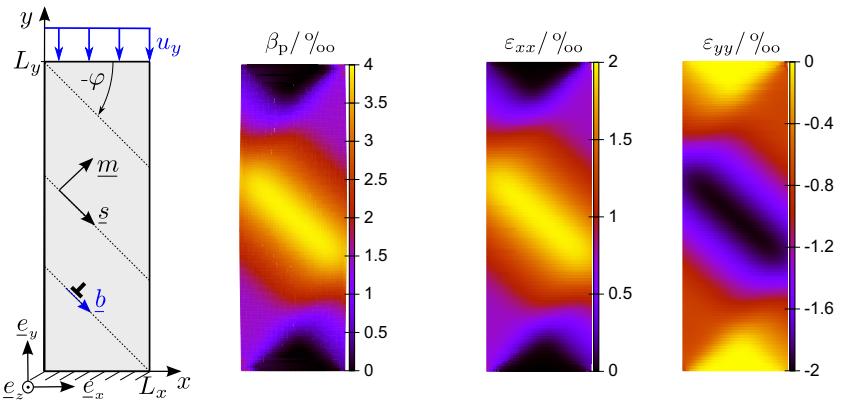

Fig. 17 From left to right: Sketch of the uniaxial compression test for $\varphi = -45°$, plastic slip field plotted on the *deformed* domain (magnified by a factor of 20), strain fields plotted on the *undeformed* domain. The final state for a total compression of $-1‰$ is shown

Table 2 Material parameters for Cu single crystals

μ/MPa	λ/MPa	τ_{cr}/MPa	b/µm	ρ_s/µm^{-2}	k
44117.65	113445.38	1.00	2.56×10^{-4}	1×10^4	6.5×10^{-4}

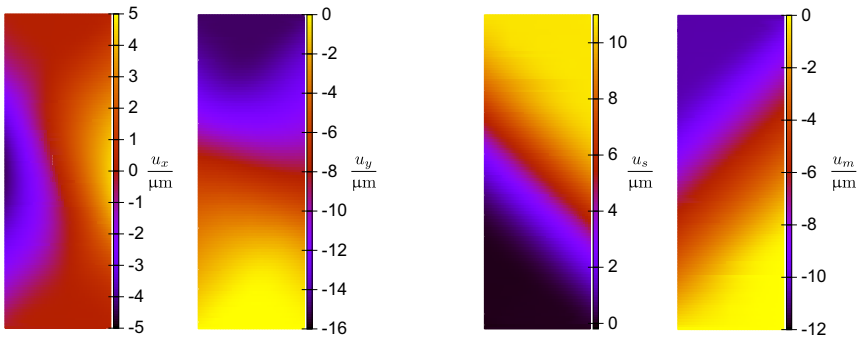

Fig. 18 Displacement field coefficients with respect to $\underline{e}_x, \underline{e}_y, \underline{s}, \underline{m}$, final state for a total compression of $-1‰$ plotted on the *undeformed* crystal domain: $u_s = \underline{u}\cdot\underline{s}$ and $u_m = \underline{u}\cdot\underline{m}$ clearly show the single-slip characteristics under $\varphi = -45°$

Further, directional derivatives are introduced as

$$u_{s,m} = \frac{\partial u_s}{\partial m} = \underline{m}\cdot(\underline{\nabla}\otimes\underline{u})\cdot\underline{s} \quad \text{and} \quad u_{m,s} = \frac{\partial u_m}{\partial s} = \underline{s}\cdot(\underline{\nabla}\otimes\underline{u})\cdot\underline{m}. \tag{87}$$

It is remarkable that despite the nonlinear distribution for $u_x(x, y)$ and $u_y(x, y)$, the fields $u_s(x, y)$ and $u_m(x, y)$ are aligned with respect to the slip direction and the slip plane normal, as shown in Fig. 18. Exactly the same behavior was observed experimentally [14].

The directional derivatives (87) contain more information about $u_s(x, y)$ and $u_m(x, y)$. Florando et al. suggested that $u_{s,m}$ is a measure of primary slip activity—here corresponding to the slip system $\underline{s}\otimes\underline{m}$—whereas $u_{m,s}$ was attributed to orthogonal slip activity [14]. This seems plausible as $u_{s,m}$ measures the *change* of the displacement in slip direction *orthogonal* to this direction, i.e., for neighboring parallel slip planes. Consequently, $u_{m,s}(x, y)$ was expected to vanish under single slip. However, the experiments showed $u_{m,s}$ to be in the same order of magnitude as $u_{s,m}$. Despite considerable effort the experimenters did not succeed in eliminating $u_{m,s}$, not even for small deformations. Thus, the nature of the apparent orthogonal slip activity remained unclear [13]. The simulation results now offer an explanation for this behavior as they confirm the experimental results *under strict single-slip conditions*, as shown in Fig. 19.

Note that derivatives $u_{s,m}$ and $u_{m,s}$ both enter PDE (61b) and (68), which hold for single slip. From a physical point of view, this results from the resolved shear stress and the symmetry of the stress tensor [cf.

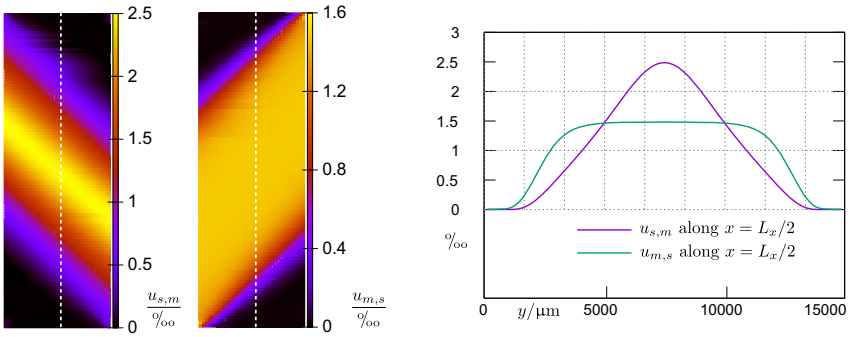

Fig. 19 Directional derivatives according to Definition (87), left: fields for a total compression of $-1‰$, right: distribution in the middle of the specimen along $x = L_x/2$ (dashed white line)

Eqs. (53)–(56) and (69)]. From a mathematical point of view, there is no reason to expect $u_{m,s}$ to *always* vanish. In summary, this means: Single slip as modeled by Constraint (50) can be accompanied by gradients $u_{s,m}$ *and* $u_{m,s}$ at the same time. Hence, it might be misleading to measure the activity of a primary and a possible orthogonal slip system *only* looking at these gradients. This conclusion agrees perfectly with the experimental results because in the Cu single crystals a slip system orthogonal to the primary one simply did not exist [14]. All in all, the simulation results confirm that the experimenters had indeed realized single-slip conditions (in the small strain regime).

Remark 5 On the length scale of the results, in order to simulate the experiment accurately, the domain's dimensions had to be chosen much larger compared to the previous examples. Consequently, the spacial discretization is too coarse to resolve any dislocation structures. Hence, the dislocation structures reported in [13,42] cannot be used for the validation of the present results as they are on a much smaller scale. In order to do so, a sub-model technique can be applied using a CDT on a finer scale, e.g., [1,32].

7 Conclusions and discussion

In this paper, the well-established continuum dislocation theory (CDT) was integrated into a general thermodynamical framework with the goal of deriving suitable field equations. In doing so, special emphasis was put on illustrating cross-references to other existing methods such as the phase field approach and potential energy minimization. It was shown under which assumptions the same field equations are obtained. Conversely, thermodynamical consequences of the rather formal phase field approach were discovered. Therefore, possible thermodynamical drawbacks and problems were discussed and remedies were offered as well. Additionally, a new *dynamic* CDT formulation was proposed. As a mathematical benefit, this form is suitable for developing numerical integration schemes. Furthermore, CDT was extended with respect to new dissipative phenomena. For some of them, a clear physical interpretation was given, whereas others must remain abstract for the moment. Still, mechanisms such as non-local dissipation could play an important role in order to describe and predict effects known from experiments. The present work thus provides a thermodynamically consistent framework of the CDT allowing comprehensive extensions.

A general point of criticism for thermodynamic approaches in higher gradient continuum theories is that the potentials and power densities of the body are somewhat uncertain. It is clear that if a thermodynamic approach is chosen—as in the present study—the form of potentials and power densities play the fundamental role in the theory, far beyond mere thermodynamic consistency. The present study pursues another intention in so far as the generic thermodynamic treatment of the CDT was used to clarify physical consequences of an existing theory. This procedure provides a basis for new extensions. Along the way it is important to adapt the form of the potentials, power densities, etc. as soon as new insights from statistical physics of dislocations are available.

Different features of the CDT were exemplified by the simulation of various plane deformation processes on Al and Cu single crystals. Thereby, only a selection of the manifold dissipative mechanisms discussed in Sect. 4.4 could be considered: If the dissipation potential depends on the rate of plastic distortion, viscoplastic behavior can be obtained. A simple quadratic form results in a linear relation between viscous stress and slip rate. More elaborate forms that even consider a bounded dislocation velocity (and thus a bounded plastic

strain rate) are conceivable as well. Of great value is the case when the dissipation potential depends both on the absolute value and on the square of the rate of plastic distortion. Then, a model can be *deduced* that shows striking analogies to phenomenological viscoplasticity such as the appearance of a Perzyna-type flow rule. Moreover, this behavior was not explicitly introduced into the model, but results naturally from the aforementioned assumptions. This offers the opportunity for physical validation of phenomenological material laws. Furthermore, the numerical studies in this work were used to analyze the effect of different boundary conditions (BCs). Shear tests with periodic BCs for both primary fields admit a homogeneous solution for the plastic distortion field. In this case, dislocation density and backstresses vanish. For this reason, no Bauschinger effect (kinematic hardening) due to backstresses was observable. Instead, a pronounced Bauschinger effect arose from the slip system orientation (Schmid's law). Confined bending tests were then used to enforce significant plastic slip gradients. The resulting dislocation structures could be interpreted as pile-ups of edge dislocations. However, a *global* effect from the corresponding backstress in the form of kinematic hardening could only be achieved using unphysically high dislocation energies. Otherwise, this higher-order effect remains almost invisible under single-slip conditions. Pure relaxation tests revealed low energy dislocation patterns in the form of band structures. These numerical results show a strong similarity to dislocation patterns obtained in DDD simulations and some similarities to experimentally observed dislocation patterns. Finally, a direct comparison to experimental field data from digital image correlation was possible for uniaxial compression tests. For the distribution of the displacement and strain fields, a striking similarity between simulation and experiment was found.

At the moment, the theory is restricted to small deformations. However, there is a lot of current work [10,21,28,34,35] guiding the way to a consistent large strain formulation. Still, some problems remain open (even for small strains). One of them, the apparent symmetry mismatch between stress and backstress tensor in Eq. $(36)_2$ from Sect. 4.4.1, was already investigated and solved [51]. The case of one active slip system is often considered because of its simplicity and clearness—as in this paper as well. However, single slip causes the plastic distortion to become highly anisotropic and hence imposes severe constraints on the crystal's behavior. Of course, this is far from the real slip behavior in many cases. A *physically consistent* extension to more than one active slip system is desirable but *not* straightforward (cf., e.g., [11]). Particularly, the formulation of the dislocation self and interaction energy is not fully clear at the moment though there are some promising approaches [12]. When slip system-dependent dislocation densities are introduced, care should be taken that the kinematics is still redundance-free [51]. Next, the 2D plane strain scenario used in this work implicitly assumes straight dislocation lines as there is no curvature of dislocations considered. In fact, there is a 3D CDT, which captures curved dislocation loops by introducing a higher space dimension [48]. However, the theoretical and computational effort seems high. The advantage of the presented CDT, in turn, is its clarity and compactness, and there are new developments into ways of including curved dislocation lines as well [34].

In future research, the *consistent* extension of the theory to several slip systems [51] and geometrical nonlinearity will be investigated. Of special importance will be the interaction of slip systems, such as cross-slip. This strongly affects the self-organized behavior and can lead to stationary dislocation structures [59]. Of utmost importance is the validation of theoretical predictions with experimental results. Though it is a challenging task, more micromechanical experiments should be conducted on such a length scale that measurements of dislocation tensor coefficients can be compared directly to numerical results [31,45]. Furthermore, it seems promising to investigate the impact of non-proportional loading on dislocation patterns in more detail. Thus, the validation of assumptions within coarser-grained models as well as a reasonable estimation of introduced microstructural material parameters will become possible [53].

Acknowledgements This research was supported by German Science Foundation (DFG) within the Collaborative Research Center SFB 692 HALS. The authors are grateful to Professor K.C. Le, Professor P. Neff, Professor M.F.-X. Wagner, Dr. Ralf Landgraf and Dr. Hendrik Donner for fruitful discussions. Moreover, the help of Hugh Wessel and the extremely constructive criticism from the reviewers is acknowledged.

Appendix A: elements of tensor calculus and tensor analysis

Especially in the context of a continuum theory, involving higher gradients of field variables, a clear, systematic, compact and consistent tensor calculus is indispensable. In the present study, an elaborate formalism [43] is adopted, which is applicable to tensor fields of *arbitrary* rank. Essential elements are briefly recapitulated in the following paragraphs.

Transposition of tensors

Transposition of tensors in the sense of this study means completely permuting the order of basis vectors. For example,

$$\underline{u}^{\mathrm{T}} = \underline{u}, \tag{88a}$$
$$(\underline{u} \otimes \underline{v})^{\mathrm{T}} = \underline{v} \otimes \underline{u}, \tag{88b}$$
$$(\underline{u} \otimes \underline{v} \otimes \underline{w})^{\mathrm{T}} = \underline{w} \otimes \underline{v} \otimes \underline{u}, \tag{88c}$$
$$(\underline{\underline{U}} \otimes \underline{\underline{V}})^{\mathrm{T}} = \underline{\underline{U}}^{\mathrm{T}} \otimes \underline{\underline{V}}^{\mathrm{T}}. \tag{88d}$$

Multiple dot products of tensors

Within this study, the following convention is used: Vertical dot products denote the contraction of adjoining basis vectors, whereas horizontal dot products denote the laterally reversed contraction of basis vectors. For example, consider a Cartesian base $\underline{e}_a = \{\underline{e}_x, \underline{e}_y, \underline{e}_z\}$ and

$$\underline{u} \cdot \underline{v} = u_a \, \underline{e}_a \cdot v_b \underline{e}_b = u_a v_a, \tag{89a}$$
$$\underline{\underline{U}} \cdot\cdot \, \underline{\underline{V}} = U_{ab} \, \underline{e}_a \otimes \underline{e}_b \cdot\cdot \, V_{cd} \, \underline{e}_c \otimes \underline{e}_d = U_{ab} V_{ba}, \tag{89b}$$
$$\underline{\underline{\underline{U}}} \cdots \underline{\underline{\underline{V}}} = U_{abc} \, \underline{e}_a \otimes \underline{e}_b \otimes \underline{e}_c \cdots V_{def} \, \underline{e}_d \otimes \underline{e}_e \otimes \underline{e}_f = U_{abc} V_{abc} \tag{89c}$$

and so on. Here, Einstein's summation convention was also applied. The multiple contraction is important for the definition of the scalar product of tensors and their norm, which has to be nonnegative. The following definitions of the Euclidean norm fulfill this requirement:

$$\|\underline{u}\| = \sqrt{\underline{u} \cdot \underline{u}^{\mathrm{T}}}, \tag{90a}$$
$$\|\underline{\underline{U}}\| = \sqrt{\underline{\underline{U}} \cdot\cdot \, \underline{\underline{U}}^{\mathrm{T}}}, \tag{90b}$$
$$\|\underline{\underline{\underline{U}}}\| = \sqrt{\underline{\underline{\underline{U}}} \cdots \underline{\underline{\underline{U}}}^{\mathrm{T}}}. \tag{90c}$$

Nabla operator

The Nabla operator is a vector-valued differential operator, which can be defined, e.g., using a Cartesian base:

$$\underline{\nabla} = \underline{e}_a \frac{\partial}{\partial x_a}, \quad \underline{\nabla}(\,) = (\,)_{,a} \, \underline{e}_a. \tag{91}$$

Right gradient

Assuming the following definitions for the total differential of a tensor field with respect to space

$$\mathrm{d}\alpha = \mathrm{grad}(\alpha) \cdot \mathrm{d}\underline{r}, \tag{92a}$$
$$\mathrm{d}\underline{u} = \mathrm{grad}(\underline{u}) \cdot \mathrm{d}\underline{r}, \tag{92b}$$
$$\mathrm{d}\underline{\underline{U}} = \mathrm{grad}(\underline{\underline{U}}) \cdot \mathrm{d}\underline{r}, \tag{92c}$$

yields a coordinate-free definition of the right gradient:

$$\mathrm{grad}(\alpha) = (\underline{\nabla} \otimes \alpha)^{\mathrm{T}} = \underline{\nabla}\alpha, \tag{93a}$$
$$\mathrm{grad}(\underline{u}) = (\underline{\nabla} \otimes \underline{u}^{\mathrm{T}})^{\mathrm{T}} = (\underline{\nabla} \otimes \underline{u})^{\mathrm{T}}, \tag{93b}$$
$$\mathrm{grad}(\underline{\underline{U}}) = (\underline{\nabla} \otimes \underline{\underline{U}}^{\mathrm{T}})^{\mathrm{T}}, \tag{93c}$$

which can be easily generalized for tensors of arbitrary order, e.g.,

$$\mathrm{d}\underline{\underline{\underline{V}}} = \mathrm{grad}(\underline{\underline{\underline{V}}}) \cdot \mathrm{d}\underline{r} = (\underline{\nabla} \otimes \underline{\underline{\underline{V}}}^{\mathrm{T}})^{\mathrm{T}} \cdot \mathrm{d}\underline{r} = (\underline{\underline{\underline{V}}} \otimes \underline{\nabla}) \cdot \mathrm{d}\underline{r}. \tag{94}$$

If the operator is to stand left of the argument (which is the traditional notation in mathematics), the depicted transposition must be used. Otherwise and only if there is no danger of confusing the argument, the operator can also be put to the right of the argument. This saves multiple transposition. As an example with Cartesian coordinates consider

$$\mathrm{grad}(\underline{\underline{U}}) = A_{ab,c}\ \underline{e}_a \otimes \underline{e}_b \otimes \underline{e}_c, \quad \mathrm{d}\underline{\underline{U}} = A_{ab,c}\ \mathrm{d}x_c\ \underline{e}_a \otimes \underline{e}_b.$$

Right divergence

Assuming Gauss' divergence theorem to be valid, i.e.,

$$\int\int\int_V \mathrm{div}(\underline{u})\ \mathrm{d}V = \int\int_A \underline{u} \cdot \underline{n}\ \mathrm{d}A, \tag{95a}$$

$$\int\int\int_V \mathrm{div}(\underline{\underline{U}})\ \mathrm{d}V = \int\int_A \underline{\underline{U}} \cdot \underline{n}\ \mathrm{d}A, \tag{95b}$$

a coordinate-free definition of the divergence of a tensor field is obtained:

$$\mathrm{div}(\underline{u}) = \lim_{V\to 0} \frac{1}{V} \int\int_A \underline{u} \cdot \underline{n}\ \mathrm{d}A, \tag{96a}$$

$$\mathrm{div}(\underline{\underline{U}}) = \lim_{V\to 0} \frac{1}{V} \int\int_A \underline{\underline{U}} \cdot \underline{n}\ \mathrm{d}A. \tag{96b}$$

The divergence can be expressed using the Nabla operator in the following ways:

$$\mathrm{div}(\underline{u}) = \mathrm{grad}(\underline{u}) \cdot\cdot\ \underline{\underline{I}} = (\underline{\nabla} \otimes \underline{u}^{\mathrm{T}})^{\mathrm{T}} \cdot\cdot\ \underline{\underline{I}} = (\underline{\nabla} \cdot \underline{u}^{\mathrm{T}})^{\mathrm{T}} = \underline{u} \cdot \underline{\nabla}, \tag{97a}$$

$$\mathrm{div}(\underline{\underline{U}}) = \mathrm{grad}(\underline{\underline{U}}) \cdot\cdot\ \underline{\underline{I}} = (\underline{\nabla} \otimes \underline{\underline{U}}^{\mathrm{T}})^{\mathrm{T}} \cdot\cdot\ \underline{\underline{I}} = (\underline{\nabla} \cdot \underline{\underline{U}}^{\mathrm{T}})^{\mathrm{T}} = \underline{\underline{U}} \cdot \underline{\nabla}. \tag{97b}$$

As examples with Cartesian coordinates consider

$$\mathrm{div}(\underline{u}) = u_{b,b}, \quad \mathrm{div}(\underline{\underline{U}}) = A_{ab,b}\ \underline{e}_a.$$

Right rotation

Assuming Stokes' circulation theorem to be valid, i.e.,

$$\int\int_A \mathrm{curl}(\underline{u}) \cdot \underline{n}\ \mathrm{d}A = \oint_C \underline{u} \cdot \underline{t}\ \mathrm{d}l, \tag{98a}$$

$$\int\int_A \mathrm{curl}(\underline{\underline{U}}) \cdot \underline{n}\ \mathrm{d}A = \oint_C \underline{\underline{U}} \cdot \underline{t}\ \mathrm{d}l, \tag{98b}$$

yields a coordinate-free definition of the curl of a tensor field:

$$\mathrm{curl}(\underline{u}) = \lim_{\Delta A\to 0} \frac{1}{\Delta A} \oint_C \underline{u} \cdot \underline{t}\ \mathrm{d}l, \tag{99a}$$

$$\mathrm{curl}(\underline{\underline{U}}) = \lim_{\Delta A\to 0} \frac{1}{\Delta A} \oint_C \underline{\underline{U}} \cdot \underline{t}\ \mathrm{d}l. \tag{99b}$$

The curl can be expressed using the Nabla operator in the following ways:

$$\mathrm{curl}(\underline{u}) = \mathrm{grad}(\underline{u}) \cdot\cdot\ \underline{\underline{\underline{\epsilon}}} = (\underline{\nabla} \otimes \underline{u}^{\mathrm{T}})^{\mathrm{T}} \cdot\cdot\ \underline{\underline{\underline{\epsilon}}} = (\underline{\nabla} \times \underline{u}^{\mathrm{T}})^{\mathrm{T}} = -\underline{u} \times \underline{\nabla}, \tag{100a}$$

$$\mathrm{curl}(\underline{\underline{U}}) = \mathrm{grad}(\underline{\underline{U}}) \cdot\cdot\ \underline{\underline{\underline{\epsilon}}} = (\underline{\nabla} \otimes \underline{\underline{U}}^{\mathrm{T}})^{\mathrm{T}} \cdot\cdot\ \underline{\underline{\underline{\epsilon}}} = (\underline{\nabla} \times \underline{\underline{U}}^{\mathrm{T}})^{\mathrm{T}} = -\underline{\underline{U}} \times \underline{\nabla}. \tag{100b}$$

As examples with Cartesian coordinates consider

$$\mathrm{curl}(\underline{u}) = -u_{a,b}\epsilon_{abc}\ \underline{e}_c, \quad \mathrm{curl}(\underline{\underline{U}}) = -\underline{e}_a \otimes A_{ab,c}\ \epsilon_{bcd}\ \underline{e}_d.$$

Useful identities

The following identities are valid for tensors of arbitrary order:

$$\operatorname{curl}(\operatorname{grad}(\underline{\underline{U}})) = \underline{\underline{0}}, \quad \operatorname{div}(\operatorname{curl}(\underline{\underline{U}})) = \underline{0}. \tag{101a}$$

Gradient fields are always curl-free and curl fields are always divergence-free.

Appendix B: second derivative of the free energy for single slip

The partial derivative of the free energy with respect to the gradient of the plastic slip is calculated. Recalling Eqs. (50), (51) and (52) and introducing the abbreviation $\alpha := \underline{s} \cdot \underline{\nabla}\beta_\mathrm{p}$ gives Eq. (58) in the following form:

$$\frac{\partial \phi}{\partial \underline{\nabla}\beta_\mathrm{p}} = \frac{\partial \alpha}{\partial \underline{\nabla}\beta_\mathrm{p}} \frac{\partial \phi}{\partial \alpha} \overset{(11)}{=} \underline{s}\, \frac{k\mu}{b\rho_\mathrm{s}} \left(1 - \frac{|\alpha|}{b\rho_\mathrm{s}}\right)^{-1} \frac{\alpha}{|\alpha|}. \tag{102}$$

Taking the divergence then yields

$$\operatorname{div}\left(\frac{\partial \phi}{\partial \underline{\nabla}\beta_\mathrm{p}}\right) = \underline{\nabla} \cdot \underline{s} \left[\frac{k\mu}{b\rho_\mathrm{s}} \underbrace{\left(1 - \frac{|\alpha|}{b\rho_\mathrm{s}}\right)^{-1}}_{f(\alpha)} \frac{\alpha}{|\alpha|} \right]. \tag{103}$$

The directional gradient is a scalar operator, denoted by $\underline{s} \cdot \underline{\nabla} := \nabla_s$. Applying the chain rule now gives:

$$\operatorname{div}\left(\frac{\partial \phi}{\partial \underline{\nabla}\beta_\mathrm{p}}\right) = \frac{k\mu}{b\rho_\mathrm{s}} \left[\frac{\alpha}{|\alpha|} \nabla_s f(\alpha) + f(\alpha) \nabla_s \left(\frac{\alpha}{|\alpha|}\right) \right]. \tag{104}$$

The first summand is found:

$$\nabla_s f(\alpha) = \nabla_s \left(1 - \frac{|\alpha|}{b\rho_\mathrm{s}}\right)^{-1} = \frac{\partial f}{\partial |\alpha|} \frac{\partial |\alpha|}{\partial \alpha} \nabla_s \alpha = \left(-f^2\right) \left(\frac{-1}{b\rho_\mathrm{s}}\right) \frac{\alpha}{|\alpha|} \nabla_s \alpha. \tag{105}$$

The second summand may be neglected due to:

$$\nabla_s \left(\frac{\alpha}{|\alpha|}\right) = \frac{1}{|\alpha|} \nabla_s \alpha + \frac{\alpha}{|\alpha|^2} \frac{\alpha}{|\alpha|} \nabla_s \alpha = \left(1 - \frac{\alpha^2}{|\alpha|^2}\right) \frac{\nabla_s \alpha}{|\alpha|} = 0 \; \forall \; \alpha \neq 0. \tag{106}$$

Hence, everywhere with $\alpha \neq 0$ we obtain:

$$\begin{aligned} \operatorname{div}\left(\frac{\partial \phi}{\partial \underline{\nabla}\beta_\mathrm{p}}\right) &= \frac{k\mu}{b\rho_\mathrm{s}} \left[\frac{\alpha}{|\alpha|} \left(\frac{f^2}{b\rho_\mathrm{s}}\right) \frac{\alpha}{|\alpha|} \nabla_s \alpha + f(\alpha) \cdot 0 \right] \\ &= \frac{k\mu}{(b\rho_\mathrm{s})^2} \frac{\alpha^2}{|\alpha|^2} f^2 \nabla_s \alpha = C \left(1 - \frac{|\alpha|}{b\rho_\mathrm{s}}\right)^{-2} \nabla_s \alpha. \end{aligned} \tag{107}$$

A smooth function with respect to the dislocation density is obtained. However, strictly speaking it is only valid for regions with $\alpha \neq 0$. In order to fulfill this requirement, dislocations must nucleate. Therefore, some energetic barrier must be overcome [38]. From a mathematical point of view, this property stems from Definition (7) in combination with the dislocation energy (11). The effect of the energetic barrier can be demonstrated analytically [38]. Numerically, it seems difficult to preserve this property. With Eq. (107) it is lost. However, if the energetic barrier is less than or equal to the dissipative threshold resulting from τ_cr, then the energetic barrier plays no role anymore and may be ignored.

References

1. Agiasofitou, E., Lazar, M.: On the nonlinear continuum theory of dislocations: a gauge field theoretical approach. J. Elast. **99**(2), 163–178 (2010)
2. Amodeo, R.J., Ghoniem, N.M.: Dislocation dynamics. ii. Applications to the formation of persistent slip bands, planar arrays, and dislocation cells. Phys. Rev. B **41**, 6968–6976 (1990)
3. Arsenlis, A., Parks, D.M.: Crystallographic aspects of geometrically-necessary and statistically-stored dislocation density. Acta Mater. **47**(5), 1597–1611 (1999)
4. Berdichevsky, V.: Continuum theory of dislocations revisited. Contin. Mech. Thermodyn. **18**(3–4), 195–222 (2006)
5. Berdichevsky, V.L.: On thermodynamics of crystal plasticity. Scripta Mater. **54**(5), 711–716 (2006)
6. Berdichevsky, V.L., Le, K.C.: Dislocation nucleation and work hardening in anti-plane constrained shear. Contin. Mech. Thermodyn. **18**(7–8), 455–467 (2007)
7. Biot, M.A.: Theory of propagation of elastic waves in a fluidsaturated porous solid. i. Lowfrequency range. J Acoust. Soc. Am. **28**(2), 168–178 (1956)
8. Bulatov, V., Cai, W.: Computer Simulations of Dislocations (Oxford Series on Materials Modelling). Oxford University Press, Oxford (2006)
9. Chiu, Y., Veyssiere, P.: Dislocation self-organization under single slip straining and dipole properties. Mater. Sci. Eng. A **483–484**, 191–194 (2008)
10. Cleja-Tigoiu, S.: Non-local elasto-viscoplastic models with dislocations in finite elasto-plasticity. Part i: constitutive framework. Math. Mech. Solids **18**(4), 349–372 (2013)
11. Cordero, N.M., Gaubert, A., Forest, S., Busso, E.P., Gallerneau, F., Kruch, S.: Size effects in generalised continuum crystal plasticity for two-phase laminates. J. Mech. Phys. Solids **58**(11), 1963–1994 (2010)
12. Dj, S., Forest, S., Jaric, J.P.: Size-dependent energy in crystal plasticity and continuum dislocation models. Proc. R. Soc. A **471**(2175), 20140,868+ (2015)
13. Field, D.P., Magid, K.R., Mastorakos, I.N., Florando, J.N., Lassila, D.H., Morris, J.W.: Mesoscale strain measurement in deformed crystals: a comparison of x-ray microdiffraction with electron backscatter diffraction. Phil. Mag. **90**(11), 1451–1464 (2010)
14. Florando, J.N., LeBlanc, M.M., Lassila, D.H.: Multiple slip in copper single crystals deformed in compression under uniaxial stress. Scr. Mater. **57**(6), 537–540 (2007)
15. Forest, S., Guéninchault, N.: Inspection of free energy functions in gradient crystal plasticity. Acta. Mech. Sin. **29**(6), 763–772 (2013)
16. Giorgi, C.: Continuum thermodynamics and phase-field models. Milan J. Math. **77**(1), 67–100 (2009)
17. Gregor, V.: Self-organization approach to cyclic microplasticity: a model of a persistent slip band. Int. J. Plast. **14**(1–3), 159–172 (1998)
18. Groma, I., Csikor, F.F., Zaiser, M.: Spatial correlations and higher-order gradient terms in a continuum description of dislocation dynamics. Acta Mater. **51**(5), 1271–1281 (2003)
19. Groma, I., Vandrus, Z., Ispanovity, P.D.: Scale-free phase field theory of dislocations. Phys. Rev. Lett. **114**(1), 015503 (2015)
20. Gurtin, M.E.: A gradient theory of single-crystal viscoplasticity that accounts for geometrically necessary dislocations. J. Mech. Phys. Solids **50**(1), 5–32 (2002)
21. Gurtin, M.E., Anand, L.: A theory of strain-gradient plasticity for isotropic, plastically irrotational materials. Part ii: finite deformations. Int. J. Plast. **21**(12), 2297–2318 (2005)
22. Hochrainer, T.: Thermodynamically consistent continuum dislocation dynamics. J. Mech. Phys. Solids **88**, 12–22 (2016)
23. Hull, D., Bacon, D.J.: Introduction to Dislocations, 5th edn. Butterworth-Heinemann, Oxford (2011)
24. Javanbakht, M., Levitas, V.I.: Phase field approach to dislocation evolution at large strains: computational aspects. Int. J. Solids Struct. **82**, 95–110 (2016)
25. Kaluza, M., Le, K.C.: On torsion of a single crystal rod. Int. J. Plast. **27**(3), 460–469 (2011)
26. Kochmann, D.M., Le, K.C.: Dislocation pile-ups in bicrystals within continuum dislocation theory. Int. J. Plast. **24**(11), 2125–2147 (2008)
27. Kossevich, A.M.: The Crystal Lattice. Wiley-VCH Verlag GmbH & Co. KGaA, Weinheim (1999)
28. Koster, M., Le, K.C., Nguyen, B.D.: Formation of grain boundaries in ductile single crystals at finite plastic deformations. Int. J. Plast. **69**, 134–151 (2015)
29. Koyama, T.: Phase field. In: Czichos, H., Saito, T., Smith, L. (eds.) Springer Handbook of Materials Measurement Methods, pp. 1031–1055. Springer, Berlin (2006)
30. Kröner, E.: The internal mechanical state of solids with defects. Int. J. Solids Struct. **29**(14–15), 1849–1857 (1992)
31. Kysar, J.W., Saito, Y., Oztop, M.S., Lee, D., Huh, W.T.: Experimental lower bounds on geometrically necessary dislocation density. Int. J. Plast. **26**(8), 1097–1123 (2010)
32. Lazar, M., Anastassiadis, C.: The gauge theory of dislocations: static solutions of screw and edge dislocations. Phil. Mag. **89**(3), 199–231 (2009)
33. Le, K.C.: Introduction to Micromechanics. Nova Science, Hauppauge (2010)
34. Le, K.C.: Three-dimensional continuum dislocation theory. Int. J. Plast. **76**, 213–230 (2016)
35. Le, K.C., Günther, C.: Nonlinear continuum dislocation theory revisited. Int. J. Plast. **53**, 164–178 (2014)
36. Le, K.C., Nguyen, B.D.: Polygonization: theory and comparison with experiments. Int. J. Eng. Sci. **59**, 211–218 (2012)
37. Le, K.C., Nguyen, Q.S.: Polygonization as low energy dislocation structure. Contin. Mech. Thermodyn. **22**(4), 291–298 (2010)
38. Le, K.C., Sembiring, P.: Analytical solution of plane constrained shear problem for single crystals within continuum dislocation theory. Arch. Appl. Mech. **78**(8), 587–597 (2008)
39. Le, K.C., Sembiring, P.: Plane constrained shear of single crystal strip with two active slip systems. J. Mech. Phys. Solids **56**(8), 2541–2554 (2008)
40. Le, K.C., Sembiring, P.: Plane constrained uniaxial extension of a single crystal strip. Int. J. Plast. **25**(10), 1950–1969 (2009)

41. Levitas, V.I., Javanbakht, M.: Thermodynamically consistent phase field approach to dislocation evolution at small and large strains. J. Mech. Phys. Solids **82**, 345–366 (2015)
42. Magid, K.R., Florando, J.N., Lassila, D.H., LeBlanc, M.M., Tamura, N., Morris, J.W.: Mapping mesoscale heterogeneity in the plastic deformation of a copper single crystal. Phil. Mag. **89**(1), 77–107 (2009)
43. Negahban, M.: Vectors and Tensors, pp. 117–167. CRC Press, Boca Raton (2012)
44. Ottosen, N.S., Ristinmaa, M.: The Mechanics of Constitutive Modeling. Elsevier, Amsterdam (2005)
45. Pantleon, W.: Resolving the geometrically necessary dislocation content by conventional electron backscattering diffraction. Scr. Mater. **58**(11), 994–997 (2008)
46. Richeton, T., Dobron, P., Chmelik, F., Weiss, J., Louchet, F.: On the critical character of plasticity in metallic single crystals. Mater. Sci. Eng. A **424**(1–2), 190–195 (2006)
47. Sandfeld, S., Monavari, M., Zaiser, M.: From systems of discrete dislocations to a continuous field description: stresses and averaging aspects. Modell. Simul. Mater. Sci. Eng. **21**(8), 085,006+ (2013)
48. Sandfeld, S., Thawinan, E., Wieners, C.: A link between microstructure evolution and macroscopic response in elasto-plasticity: formulation and numerical approximation of the higher-dimensional continuum dislocation dynamics theory. Int. J. Plast. **72**, 1–20 (2015)
49. Shutov, A.V., Ihlemann, J.: A viscoplasticity model with an enhanced control of the yield surface distortion. Int. J. Plast. **39**, 152–167 (2012)
50. Shutov, A.V., Kreißig, R.: Finite strain viscoplasticity with nonlinear kinematic hardening: phenomenological modeling and time integration. Comput. Methods Appl. Mech. Eng. **197**(21–24), 2015–2029 (2008)
51. Silbermann, C.B., Ihlemann, J.: Kinematic assumptions and their consequences on the structure of field equations in continuum dislocation theory. IOP Conf. Ser. Mater. Sci. Eng. **118**, 012,034+ (2016)
52. Silbermann, C.B., Ihlemann, J.: Analogies between continuum dislocation theory, continuum mechanics and fluid mechanics. IOP Conf. Ser. Mater. Sci. Eng. **181**, 012,037+ (2017)
53. Silbermann, C.B., Shutov, A.V., Ihlemann, J.: Modeling the evolution of dislocation populations under non-proportional loading. Int. J. Plast. **55**, 58–79 (2014)
54. Ván, P., Berezovski, A., Papenfuss, C.: Thermodynamic approach to generalized continua. Contin. Mech. Thermodyn. **26**(3), 403–420 (2014)
55. Walgraef, D.: Spatio-Temporal Pattern Formation. Springer, New York (1997)
56. Wang, Y.U., Jin, Y.M., Cuitiño, A.M., Khachaturyan, A.G.: Nanoscale phase field microelasticity theory of dislocations: model and 3d simulations. Acta Mater. **49**(10), 1847–1857 (2001)
57. Wriggers, P.: Solution methods for time independent problems. In: Nonlinear Finite Element Methods, pp. 149–204. Springer Heidelberg (2008)
58. Wulfinghoff, S., Forest, S., Böhlke, T.: Strain gradient plasticity modeling of the cyclic behavior of laminate microstructures. J. Mech. Phys. Solids **79**, 1–20 (2015)
59. Xia, S., El-Azab, A.: Computational modelling of mesoscale dislocation patterning and plastic deformation of single crystals. Modell. Simul. Mater. Sci. Eng. **23**(5), 055,009+ (2015)
60. Zahn, D., Tlatlik, H., Raabe, D.: Modeling of dislocation patterns of small- and high-angle grain boundaries in aluminum. Comput. Mater. Sci. **46**(2), 293–296 (2009)